Elsevier Editorial System(tm) for Journal of Colloid and Interface Science
Manuscript Draft

Manuscript Number: JCIS-20-2315R1

Title: Tuning wall thickness of TiO_2 microtubes for an enhanced photocatalytic activity with thickness-dependent charge separation efficiency

Article Type: Full length article

Section/Category: C. Adsorption, Catalysis and Electrochemistry

Keywords: Electrospinning; TiO_2; Microtube; Wall thickness; Thickness-dependent; Photocatalysis

Corresponding Author: Professor Zhi-Gang Chen, Ph.D.

Corresponding Author's Institution: University of Southern Queensland

First Author: Xinxin Zou

Order of Authors: Xinxin Zou; Yanling Yang; Huajun Chen; Xiao-Lei Shi; Guoquan Suo; Xiaohui Ye; Li Zhang; Xiaojiang Hou; Lei Feng; Zhi-Gang Chen, Ph.D.

Abstract: TiO_2 microtubes with tunable wall thickness have been synthesized by a one-step electrospinning method linked with a calcination process. The wall thickness of TiO_2 microtubes can be easily tuned by altering the dosage of liquid paraffin. The influence of the thickness on the light-harvesting ability and separation efficiency of the photogenerated carriers was studied using ultraviolet-visible (UV-vis) diffuse reflectance spectroscopy, photoluminescence emission spectroscopy, and photocurrent density measurements. Results show that TiO_2 microtubes with an appropriate thickness exhibit enhanced light scattering effect, UV-vis light-harvesting ability, charge separation efficiency, and photocatalytic performance. The degradation rates of rhodamine B and 2,4-dinitrophenol by using TiO_2 microtubes synthesized at a dosage of 0.14 g/mL liquid paraffin are 99.9 % within 60 minutes and 97.8 % within 40 minutes, respectively, which are higher than most of the reported values. All these results suggest that our work provides an ideal strategy for adjusting the wall thickness of TiO_2 microtubes and new approach to enhance the photocatalytic performance of TiO_2.

CENTRE FOR FUTURE MATERIALS
Prof. Dr. Zhi-Gang Chen
Professor (Energy Materials)
PHONE +61 74631336; +61 423324518 | FAX +61 746312110
EMAIL zhigang.chen@usq.edu.au

UNIVERSITY OF SOUTHERN QUEENSLAND

18th, June 2020

Dear editor,

With this letter, I am submitting a revised manuscript entitled "**Tuning wall thickness of TiO_2 microtubes for an enhanced photocatalytic activity with thickness-dependent charge separation efficiency**" for your assessment for publication in ***Journal of Colloid and Interface Science***. I certify that this is an original manuscript that has not been submitted elsewhere for publication.

We have carefully revised the manuscript according to your and reviewers' comments. The revised parts have been marked as red color in the manuscript, and the responses to the reviewers have also been submitted as a single word file. Besides, we also checked and revised the minor mistakes in references.

Thank you for your time with this submission and I look forward to hearing good news from you.

Zhigang Chen

University of Southern Queensland

Response to comments of Reviewer 1

General Comment: The paper investigated the preparation and photocatalytic performance of TiO_2 nanotubes. The corresponding researches about TiO_2 photocatalysts were too massive, and this paper didn't exhibit high novelty. Therefore, this work may be suitable for publication after carefully address the following questions and comments.

Comment 1: The authors said "The electrospinning and the dosage of liquid paraffin can affect the wall thickness of TiO_2 nanotubes". But the effect of electrospinning has not been discussed.

Response: We greatly appreciate the positive comments and helpful suggestions.

We redefine our products as TiO_2 microtubes because of the size at micro level. In our study, we use the same electrospinning conditions to prepare TiO_2 microtubes, and the effect of electrospinning hasn't been carried out. Therefore, we revised "The electrospinning and the dosage of liquid paraffin can affect the wall thickness of TiO_2 nanotubes" as "The dosage of liquid paraffin can affect the wall thickness of TiO_2 microtubes" on Page 7 of the revised manuscript.

Comment 2: The homogeneity of samples should be provided by the low magnification SEM images.

Response: We have added the low magnification SEM images to characterize the uniformity of the samples, as shown in **Fig. R1**. Correspondingly, we have added the following discussions as “As can be seen, the microtubes are randomly distributed, and their diameter is at a level of ~1μm.” on Page 7 of the revised manuscript.

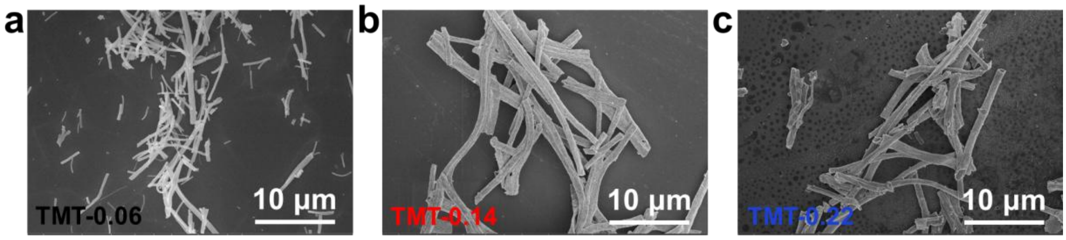

Fig. R1. (a-c) are low magnification SEM images of TMT-0.06, TMT-0.14, and TMT-0.22 samples, respectively.

The related **Fig. R1** has been supplemented in **Fig. 1** of the revised manuscript.

Comment 3: In manuscript, the label color of samples should be confirmed.

Response: We have relabeled the color of **Fig. R2** (Fig. 1 of the revised manuscript).

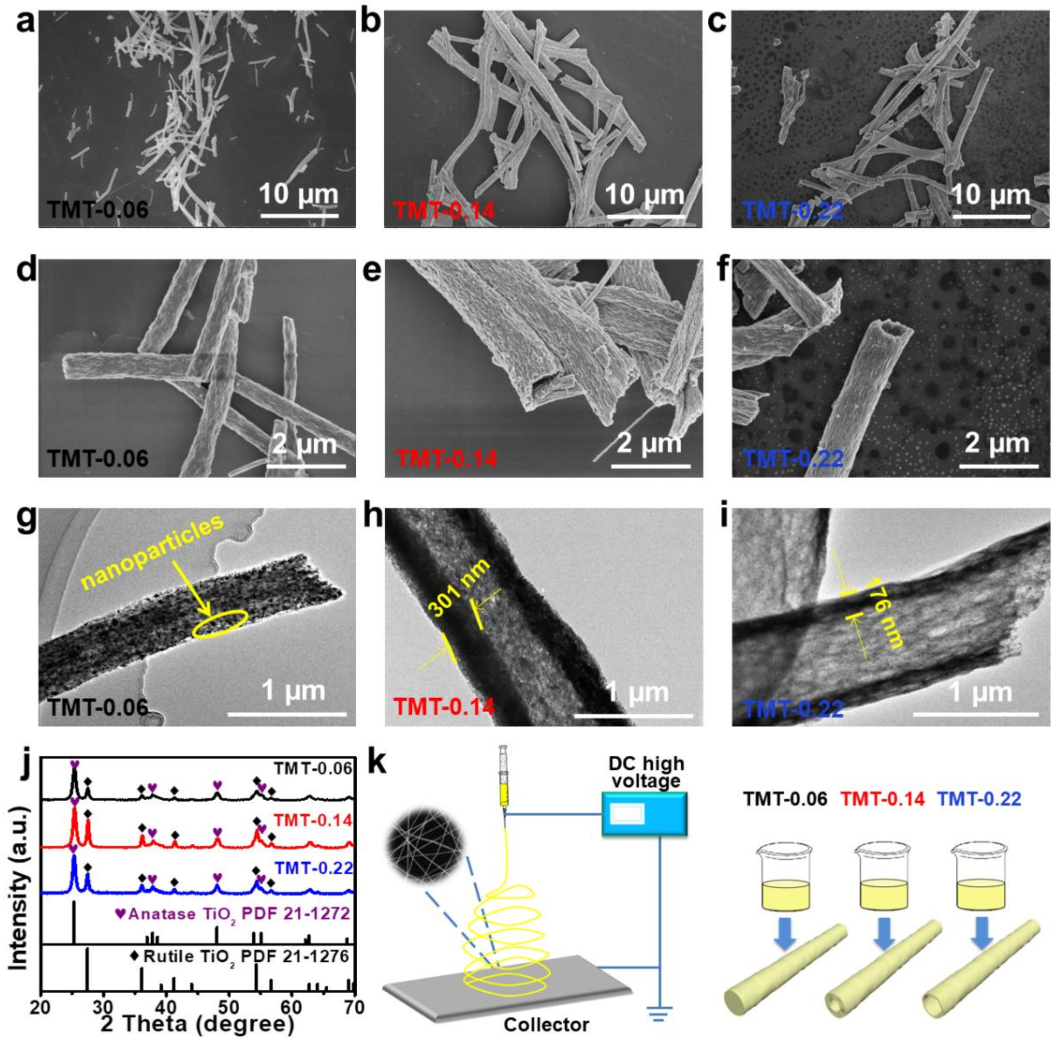

Fig. R2. SEM and TEM images of (a, d, g) TMT-0.06, (b, e, h) TMT-0.14, (c, f, i) TMT-0.22. (j) XRD patterns of TMT-0.06, TMT-0.14, and TMT-0.22. (k) Schematic diagram of synthesizing process using electrospinning and the effect of the dosage of liquid paraffin on the wall thickness of TiO_2 microtubes.

Comment 4: Whether the reproducibility and storage stability of the photocatalyst was confirmed? And what is the optimum dosage concentration of the catalyst in photocatalytic experiment?

Response: From our repeated and long-time experiments, we found that our fabricated catalysts have a good reproducibility and storage stability. The catalysts can be storage in the air. The increase of the dosage of catalyst can increase the processing cost. When the concentration of the catalyst increases to the dosage described on Page 6 of the revised manuscript, an optimal catalytic effect can be achieved. Therefore, the optimum dosage concentration of the catalyst is 0.1 g/L.

Comment 5: The photocatalytic mechanism about scattered light and secondary absorption wasn't reliably. Provide more characterization.

Response: To further clarify the photocatalytic mechanism on scattered light and secondary absorption, we added more detailed discussions and evidences as "There are a lot of void spaces in the hollow structure, which are easy to produce light-trapping effect [1]. After light penetrates into the wall of TiO_2 microtubes, the incident light is scattered multiple times within the microtubes as shown in **Fig. 5**. The microtube has secondary absorption of the scattered light to enhance the light-harvesting and improve the utilization of the incident light. This behavior is similar to the report in multiple shell CeO_2 hollow microspheres [2]." on Page 14 in the revised manuscript.

Comment 6: The large tube diameter and length inversely reduce the specific surface area. Please comparing with the TiO_2 nanotube arrays. The following papers about TiO_2 nanotube arrays also reported the photocatalytic degradation of dyes, please reference and cite them. Sep. Purif. Technol., 2018, 207, 206-212; Electrochim. Acta, 330 (2020) 135167; J. Colloid Interf. Sci., 2019, 556, 92-101; Sep. Purif. Technol., 2019, 215, 565-572; Sep. Purif. Technol., 2019, 209, 782-788.

Response: We have cited the mentioned references in introduction on Page 4 of the revised manuscript. We also compare our results with the mentioned references reported TiO_2 nanotube arrays as shown in **Fig. R3** and added the discussions "the comparison of the degradation rates of TMT-0.14 in this work and other reports is shown in **Fig. 4c**. Obviously, the degradation rate of TMT-0.14 prepared herein is superior to most of the TiO_2 nanotube array composites [3] and TiO_2 nanotube composites [4-7] reported in the literature" on Page 12 of the revised manuscript.

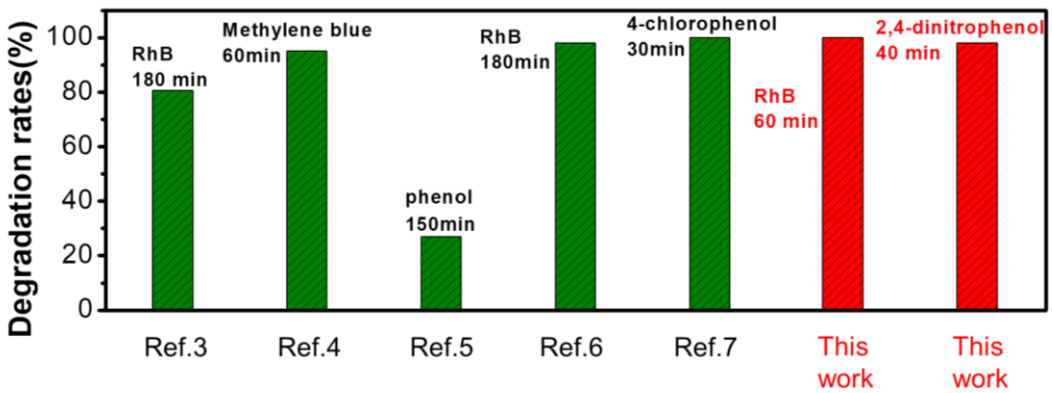

Fig. R3. Comparison of the degradation rates of TMT-0.14 in this work and other reports.

References

[1] G. Prieto, H. Tuysuz, N. Duyckaerts, J. Knossalla, G.-H. Wang, F. Schuth, Hollow nano- and microstructures as catalysts, Chem. Rev. 116 (2016) 14056-14119.9.

[2] J. Qi, K. Zhao, G. Li, Y. Gao, H. Zhao, R. Yu, Z. Tang, Multi-shelled CeO_2 hollow microspheres as superior photocatalysts for water oxidation, Nanoscale 6 (2014)

4072-4077.

[3] Q. Wang, H. Li, X. Yu, Y. Jia, Y. Chang, S. Gao, Morphology regulated Bi_2WO_6 nanoparticles on TiO_2 nanotubes by solvothermal Sb^{3+} doping as effective photocatalysts for wastewater treatment, Electrochim Acta. 330 (2020) 135167.

[4] U. Alam, M. Fleisch, I. Kretschmer, D. Bahnemann, M. Muneer, One-step hydrothermal synthesis of Bi-TiO_2 nanotube/graphene composites: an efficient photocatalyst for spectacular degradation of organic pollutants under visible light irradiation, Appl. Catal. B-Environ. 218 (2017) 758-769.

[5] H. Wang, Y. Liang, L. Liu, J. Hu, W. Cui, Highly ordered TiO_2 nanotube arrays wrapped with g-C_3N_4 nanoparticles for efficient charge separation and increased photoelectrocatalytic degradation of phenol, J. Hazard. Mater. 344 (2018) 369-380.

[6] J. Bi, X. Huang, J. Wang, T. Wang, H. Wu, J. Yang, H. Lu, H. Hao, Oil-phase cyclic magnetic adsorption to synthesize Fe_3O_4@C@TiO_2-nanotube composites for simultaneous removal of Pb(II) and Rhodamine B, Chem. Eng. J. 366 (2019) 50-61.

[7] J. Lim, Y. Yang, M.R. Hoffmann, Activation of peroxymonosulfate by oxygen vacancies-enriched cobalt-doped black TiO_2 nanotubes for the removal of organic pollutants, Environ. Sci. Technol. 53 (12) (2019) 6972-6980.

*3: Graphical Abstract

Graphical Abstract

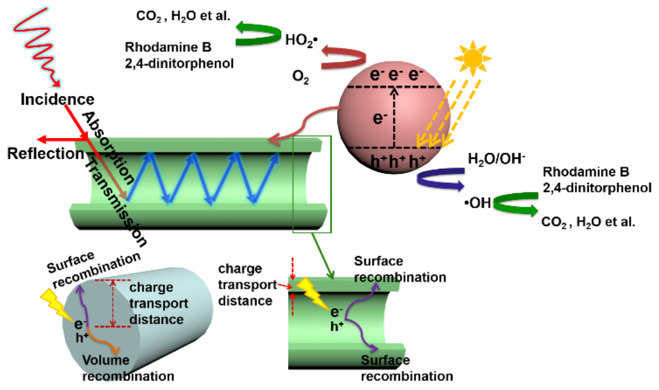

*4a: Marked highlighted manuscript

Tuning wall thickness of TiO_2 microtubes for an enhanced photocatalytic activity with thickness-dependent charge separation efficiency

Xinxin Zou[1,a], *Yanling Yang*[1,a,*], *Huajun Chen*[1,2], *Xiao-Lei Shi*[3,4], *Guoquan Suo*[1], *Xiaohui Ye*[1], *Li Zhang*[1], *Xiaojiang Hou*[1], *Lei Feng*[1], *Zhi-Gang Chen*[3,4,*]

[1]School of Materials Science and Engineering, Shaanxi Key Laboratory of Green Preparation and Functionalization for Inorganic Materials, Shaanxi University of Science and Technology, Xi'an 710021, PR China

[2]Department of Environment and Chemistry, Luoyang Institute of Science and Technology, Luoyang 471023, PR China

[3]Centre for Future Materials, University of Southern Queensland, Springfield Central, QLD 4300, Australia.

[4]School of Mechanical and Mining Engineering, The University of Queensland, QLD 4072, Australia

[a] The first two authors contributed equally to this work

Corresponding Authors

* Yanling Yang: yangyanling@sust.edu.cn.

* Zhi-Gang Chen: zhigang.chen@usq.edu.au; zhigang.chen@uq.edu.au.

ABSTRACT

TiO_2 microtubes with tunable wall thickness have been synthesized by a one-step electrospinning method linked with a calcination process. The wall thickness of TiO_2 microtubes can be easily tuned by altering the dosage of liquid paraffin. The influence of the thickness on the light-harvesting ability and separation efficiency of the photogenerated carriers was studied using ultraviolet-visible (UV-vis) diffuse reflectance spectroscopy, photoluminescence emission spectroscopy, and photocurrent density measurements. Results show that TiO_2 microtubes with an appropriate thickness exhibit enhanced light scattering effect, UV-vis light-harvesting ability, charge separation efficiency, and photocatalytic performance. The degradation rates of rhodamine B and 2,4-dinitrophenol by using TiO_2 microtubes synthesized at a dosage of 0.14 g/mL liquid paraffin are 99.9 % within 60 minutes and 97.8 % within 40 minutes, respectively, which are higher than most of the reported values. All these results suggest that our work provides an ideal strategy for adjusting the wall thickness of TiO_2 microtubes and new approach to enhance the photocatalytic performance of TiO_2.

Keywords: Electrospinning, TiO_2, Microtube, Wall thickness, Thickness-dependent, Photocatalysis

1. Introduction

With ever-increasing human activities, environmental pollution has been considered as a common challenge. Over the last decades, extensive studies have concentrated on developing high-efficiency photocatalysts including TiO_2 [1], ZnO [2], ZnS [3], CdS [4], WO_3 [5], Bi_2O_3 [6], SnO_2 [7], and g-C_3N_4 [8], to degrade the organic contaminants in wastewater [9]. Due to the unique advantages of TiO_2, such as high chemical stability, nontoxicity, controllable structure/morphology, and economic effectiveness [10], TiO_2-based photocatalysts are among the most extensively investigated [11]. Nevertheless, its wide band gap (approximately 3.2 eV) limits the light absorption in the visible-light region and severely constrain its application of TiO_2. Furthermore, the lower separation efficiency of the photogenerated carriers adversely affects the photocatalytic activity of TiO_2.

To enhance the photocatalytic activity of TiO_2-based materials, several strategies including morphology control [12], metal or non-metal doping [13], heterojunction [14], and the use of cocatalysts [15], have been developed. Particularly, the microstructures of photocatalysts have a significant influence on their light-absorption ability and charge separation efficiency [16]. It has been reported that the hollow structures show multiple light scattering [17] and enhanced solar-energy conversion efficiency [18]. Therefore, the hollow structure of TiO_2 microtubes can shorten the migration distance of the photogenerated carriers, leading to a remarkable suppression of charge recombination [19]. In addition, the large specific surface area of TiO_2 microtubes provides plentiful reactive sites, which can be used to adsorb reactant molecules.

To date, TiO_2 nano/microtubes have been fabricated using template-assisted techniques [20], solvothermal method [21], hydrothermal method [21], and electrochemical anodic oxidation [22]. However, post-treatment of template-assisted techniques, such as high-temperature annealing or acid/alkali treatments, can easily destroy the microstructure of TiO_2 nano/microtubes [23]. The reaction time of the solvothermal and hydrothermal methods can significantly affect the morphology and wall thickness of nano/microtubes and the large-scale preparation induces non-uniform size [21]. Electrochemical anodic oxidation is commonly used to prepare nanotubes. Qiu, Liu, and Zhao et al. successfully prepared TiO_2 nanotube arrays using the electrochemical anodic oxidation technology [22,24-26]. However, the type and concentration of electrolyte, pH value and temperature significantly affect the morphology of nanotubes [27]. Therefore, achieving a controllable wall thickness of TiO_2 nano/microtubes is still challenging. Compared with the above methods, the electrospinning technique can easily control the microstructure of continuous nano/microtubes and offer advantages such as flexibility, cost-effectiveness, and polymer versatility [28]. However, adjusting the wall thickness of the prepared TiO_2 nano/microtubes by the electrospinning technique remains a challenge.

In this work, we realize the controlling of the wall thickness in TiO_2 microtubes using a one-step electrospinning technique by simply varying the dosage of liquid paraffin. The morphologies, light-harvesting abilities, separation efficiencies of photogenerated carriers, and photocatalytic activities along with the photocatalytic mechanism of TiO_2 microtubes with tunable wall thickness are investigated in detail. TiO_2 microtubes with tunable wall thickness can balance light-harvesting and efficiently utilize photogenerated charge carriers and possess improved light-harvesting ability and solar-energy conversion efficiency. An appropriate wall thickness can shorten the distance of charge-migration and benefit the separation of photogenerated carriers during the photocatalytic process, resulting in a superior photocatalytic degradation.

2. Experimental

2.1 Materials

Polyvinylpyrrolidone (PVP, Mw = 1300000), butyl titanate ($C_{16}H_{36}O_4Ti$), acetylacetone ($C_5H_8O_2$), anhydrous ethanol (C_2H_5OH), and liquid paraffin were purchased from Shanghai Macklin Biochemical Co., Ltd. All the reagents used to prepare TiO_2 microtubes are of analytic grade, without additional purification.

2.2 Fabrication of TiO_2 microtubes

TiO_2 microtubes were prepared using the electrospinning technique. First, PVP (1.2 g) was dissolved in 10 mL anhydrous ethanol under magnetic stirring. Then, anhydrous ethanol, acetylacetone, and butyl titanate were mixed with 1:1:1 mass ratio and then added into 5 mL PVP solution to obtain a clear solution. Finally, different dosages of liquid paraffin were added to the 5 mL mixed solution. After magnetic stirring for 48 h, viscous solutions were obtained.

The electrospinning apparatus comprises a high voltage power supply that generates an electric field of 0-30 kV, a syringe with an inner diameter of 0.6 mm at the capillary tip, and a micro-injection pump. A high voltage (18 KV) was employed, while the distance was 20 cm between the capillary tip and the aluminum foil collector. The solution was injected (using the micro-injection pump) at a constant rate of 0.3 mL/h and collected using aluminum foil. After electrospinning, layers of white fibers on the aluminum foil were collected and then calcined at 500 ℃ for 4 hours in air at a heating rate of 5 ℃/min. The obtained powder samples of TiO_2 microtubes were finally collected and treated with different dosages of liquid paraffin. The as-prepared TiO_2 microtubes using different liquid paraffin dosages were labeled as TMT-0.06, TMT-0.14, and TMT-0.22 (where TMT is the abbreviation for TiO_2 microtubes, and the subsequent digits show the dosage of liquid paraffin used; for instance, TMT-0.06 describes the TiO_2-microtube sample prepared by adding 0.06 g liquid paraffin to 1 mL mixed solution).

2.3 Characterization of photocatalysts

The morphology and structure of TiO_2 microtubes were studied using scanning electron microscopy (SEM, FEI Verios 460, USA), transmission electron microscopy (TEM, FEI Tecnai G2 F20 S-TWIN, USA), X-ray diffraction (Rigaku D/max2200Pc, Japan) using Cu-Kα radiation (λ = 1.5406 Å) with 2θ ranging from 20° to 70°, ultraviolet-visible (UV-vis) diffuse reflection spectroscopy (Agilent CARY 5000, USA) with an integrated sphere attachment ranging from 200 to 800 nm, and photoluminescence emission spectroscopy (F-7000, Hitachi, Japan).

Photoluminescence spectra were acquired using a fluorescence spectrophotometer (F-4500, Hitachi, Japan) at an excitation wavelength of 320 nm; the width of the slits for excitation and emission were both 5 nm. The photocurrents were obtained using an electrochemical analyzer (CHI 660D, China). Photocurrent measurements on the TiO_2 microtubes were performed on a CHI660E electrochemical workstation at room temperature using a standard three-electrode cell setup containing a platinum wire, saturated calomel electrode (SCE), and TiO_2 microtubes as the counter, reference, and working electrodes, respectively. Sodium sulfate solutions were used as electrolytes.

2.4 Photocatalytic experiment

The photocatalytic activity of TiO_2 microtubes was investigated by degrading organic solutions containing rhodamine B and 2, 4-dinitrophenol (15 mg/L) under simulated solar light (CDM-T 70W/942, Philips). First, 0.01 g samples were dispersed in 100 mL organic solution (15 mg/L) at a TiO_2-microtube concentration of 0.1 g/L. After ultrasonic dispersion for 10 minutes, the suspension was stirred 30 minutes in the dark to achieve the equilibrium of absorption-desorption among the photocatalyst and the organics. Afterwards, the blend containing the photocatalyst and organic solution was irradiated with simulated solar light. At certain time intervals, the mixture was centrifuged, and the residual organics were analyzed by UV-vis absorption spectroscopy.

During the photocatalytic process, the concentrations of rhodamine B and 2,4-dinitrophenol were periodically determined via spectrophotometry. The degradation rates of rhodamine B and 2,4-dinitrophenol were calculated using Eq. (1) : [1]

$$Degradation\ Rate = \frac{c_0 - c_t}{c_0} \times 100\ \% \qquad (1)$$

where c_0 (mg/L) and c_t (mg/L) are the concentrations of rhodamine B and 2,4-dinitrophenol at time 0 and time *t*, respectively. The degradation rates of rhodamine B and 2, 4-dinitrophenol was described using a pseudo-first-order kinetics Eq. (2):

$$ln\frac{c_t}{c_0} = -k \times t \quad (2)$$

where k is the first-order kinetic rate constant of rhodamine B and 2,4-dinitrophenol during the photocatalytic process.

3. Results and discussion

Fig. 1a-c and **1d-f** show typical low/high magnification SEM images of the as-prepared TMT-0.06, TMT-0.14, and TMT-0.22, respectively. As can be seen, the microtubes are randomly distributed, and their diameter is at a level of ~1μm. The morphology of TMT-0.06 is fiber-like (**Fig. 1d**), while TMT-0.14 (**Fig. 1e**) and TMT-0.22 (**Fig. 1f**) are hollow tubulars, indicating that TiO_2 microtubes can be successfully prepared by adding liquid paraffin. Moreover, many wrinkles appear on the surface of TiO_2 microfibers or microtubes due to the volatilization of liquid paraffin. To confirm the hollow structure of TiO_2, the microstructure and wall thickness of TiO_2 microtubes were also estimated by using TEM and shown in **Fig. 1g-i**. At a dosage of 0.06 g/mL, the sample consists of nanoparticles and exhibits a well-defined porous structure (**Fig. 1g**). Upon increasing the amount of liquid paraffin to 0.14 and 0.22 g/mL, a hollow structural morphology of TiO_2 microtubes can be observed. Besides, the wall thickness of TiO_2 microtubes decreases with the addition of liquid paraffin. When the dosages of liquid paraffin are 0.14 and 0.22 g/mL, the wall thickness of TiO_2 microtubes can be measured to be ~300 and 180 nm, respectively (**Fig. 1h-i**). The dosage of liquid paraffin can affect the wall thickness of TiO_2 microtubes. At high liquid paraffin concentrations, the liquid paraffin on the fiber surface volatilizes in the presence of anhydrous ethanol, thus promoting the aggregation of PVP and butyl titanate on the fiber surface. The remaining liquid paraffin is slowly separated from the remaining solvent and accumulates inside the fiber during the drying process [29]. The decrease in wall thickness may be triggered by volatilization of more liquid paraffin at high temperatures during calcination. These SEM and TEM results show that the morphology of TiO_2 microtubes can be tuned by controlling the dosage of liquid paraffin, indicating that our synthesis strategy has high controllability of the wall thickness in TiO_2 microtubes. **Fig. 1j** presents the XRD patterns of TiO_2 microtubes synthesized at different dosages of liquid paraffin. As can be seen, all samples comprised mixed anatase (JCPDS card No. 21-1272) and rutile TiO_2 (JCPDS card No. 21-1276), indicating that anatase/rutile homojunctions are existed in the as-prepared TiO_2 microtubes. In order to illustrate the effect of the dosage of liquid paraffin on the wall thickness of TiO_2 microtubes, a sketch map of fabrication of TiO_2 microtubes is schematically shown in **Fig. 1k**, where the liquid paraffin acts as soft template for the controlling of the wall thickness in TiO_2 microtubes.

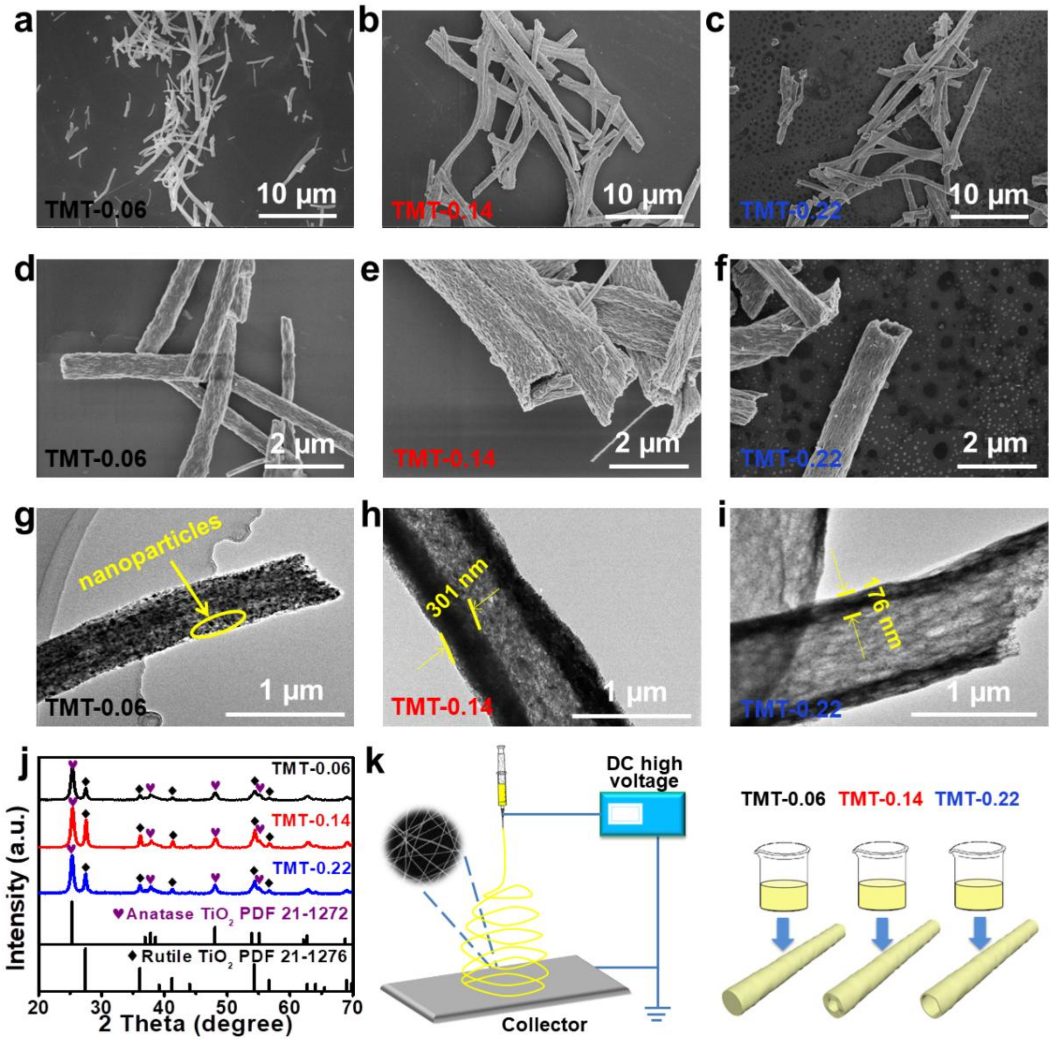

Fig. 1. SEM and TEM images of (a, d, g) TMT-0.06, (b, e, h) TMT-0.14, (c, f, i) TMT-0.22. (j) XRD patterns of TMT-0.06, TMT-0.14, and TMT-0.22. (k) Schematic diagram of synthesizing process using electrospinning and the effect of the dosage of liquid paraffin on the wall thickness of TiO_2 microtubes.

To evaluate the optical absorptivity of the as-prepared TMT-0.06, TMT-0.14, and TMT-0.22, a UV-vis diffuse reflectance spectroscopy was performed, and the results are shown in **Fig. 2a**. As can be seen, the optical absorptivity is increasing from TMT-0.06 to TMT-0.14 and then decreasing slightly for TMT-0.22, indicating that TMT-0.14 has a suitable wall thickness and the incident light can strongly scatter inside the microtubes of TMT-0.14, causing secondary absorption of the scattered light and increasing the optical absorptivity [30]. The microtube wall becomes thinner as the dosage of liquid paraffin continues to increase, and the hollow structure becomes more pronounced. Compared with TMT-0.14, TMT-0.22 shows a decreased optical absorptivity, suggesting that reducing the wall thickness increases the transmittance of the incident light, resulting in a weaker light scattering effect and thereby reducing light-harvesting activity [18].

Fig. 2b plots the optical band gap of the as-prepared TMT-0.06, TMT-0.14, and TMT-0.22 and shows that the optical band gaps of the TMT-0.06, TMT-0.14 and TMT-0.22 are 3.20, 3.10 and 3.15 eV, respectively. The measured band gap of all our samples is very close to that of anatase TiO_2 (3.2 eV). The slightly decreased band gap is caused by the distinct of hollow microstructures and the presence of rutile TiO_2 in the samples [29], indicating that a suitable hollow structure is conducive to reducing the band gap. **Fig. 2c** shows the photoluminescence emission spectra of the as-prepared TMT-0.06, TMT-0.14, and TMT-0.22 under ultraviolet excitation at 320 nm. TMT-0.14 exhibits a lower photoluminescence intensity compared to TMT-0.06, suggesting that the tubular structure of the microtubes can suppress the recombination of photogenerated carriers (excitation of TiO_2 under ultraviolet light). Actually, the tubular structure of the microtubes can largely shorten the migration distance of the photogenerated electrons and holes, and reduce the recombination of photogenerated carriers and improving the photocatalytic efficiency [19], However, excessive liquid paraffin addition (such as 0.22 g/mL) results in higher photoluminescence intensity of TMT-0.22 because the thin wall may reduce the charge-driving force and weaken the separation and transfer of charge, which is harmful to the suppression of photogenerated carrier recombination [31].

Fig. 2d shows the photocurrent response of the as-prepared TMT-0.06, TMT-0.14, and TMT-0.22 to the solar-simulated light irradiation of 0.1 M Na_2SO_4 electrolyte at the voltage of 0.1 V. With increasing the concentration of liquid paraffin, the photocurrent density of TMT-0.14 is greater than TMT-0.06 and the photocurrent density of TMT-0.22 decreases slightly. The results of the photocurrent measurements suggest that TMT-0.14 has a suitable wall thickness, which is favorable for an improved light-absorption capability and plays an important role in the generation of photocurrent. However, the thinner wall thickness of TMT-0.22 did not correspond to better photocurrent density. If the wall thickness is below the width of the space-charge layer, the band bending is reduced [18] and the electric driving force is decreased, which deteriorates the separation and transfer of photogenerated carriers [32].

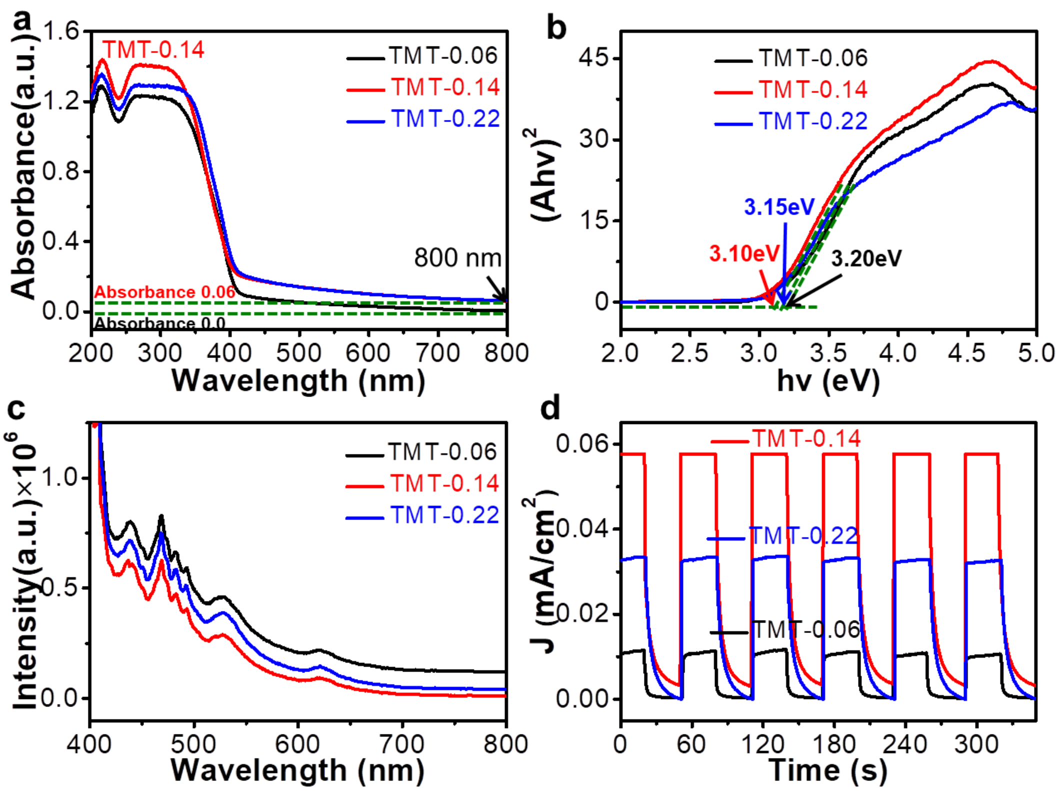

Fig. 2. UV-vis diffuse reflectance spectra, photoluminescence spectra, and photocurrent of TiO_2 microtubes of TMT-0.06, TMT-0.14, and TMT-0.22. (a) UV-vis diffuse reflectance spectra. (b) Optical band gap energy of TMT-0.06 TMT-0.14, and TMT-0.22. (c) Photoluminescence emission spectra excited under 320 nm UV light. (d) The photocurrent of TiO_2 microtubes with tunable wall thickness under the irradiation of solar-simulated light, Pt-wire is counter electrode, constant bias vs. SCE is 0.1 V, and the working electrode is 3.5 cm×1.0 cm in size.

The photocatalytic activities of as-prepared TiO_2 microtubes were further evaluated by the photocatalytic degradations of rhodamine B and 2,4-dinitrophenol under simulated solar-light irradiation. **Fig. 3** shows the degradation processes and kinetics for rhodamine B and 2,4-dinitrophenol using TMT-0.06, TMT-0.14, and TMT-0.22. **Fig. 3a** shows that the degradation rate of photocatalytic of TMT-0.14 is 99.9 % after 60 minutes. **Fig. 3b** plots the degradation kinetics of rhodamine B for TMT-0.06, TMT-0.14, and TMT-0.22 and shows first-order kinetics. **Fig. 3c** shows the degradation processes of 2,4-dinitrophenol by TMT-06, TMT-0.14, and TMT-0.22. After 40 minutes of simulated solar-light irradiation, the photocatalytic degradation rates of TMT-0.06, TMT-0.14, and TMT-0.22 are 92.8 %, 97.8 %, and 95.2 %, respectively. **Fig. 3d** shows the degradation kinetics of 2,4-dinitrophenol for TMT-0.06, TMT-0.14, and TMT-0.22, which are also consistent with first-order kinetics. These results show that the catalytic activity of TiO_2 microtubes with different wall thickness is different, which should be attributed to their effects on the charge separation efficiency, specific surface area [32], and light-harvesting capability [33].

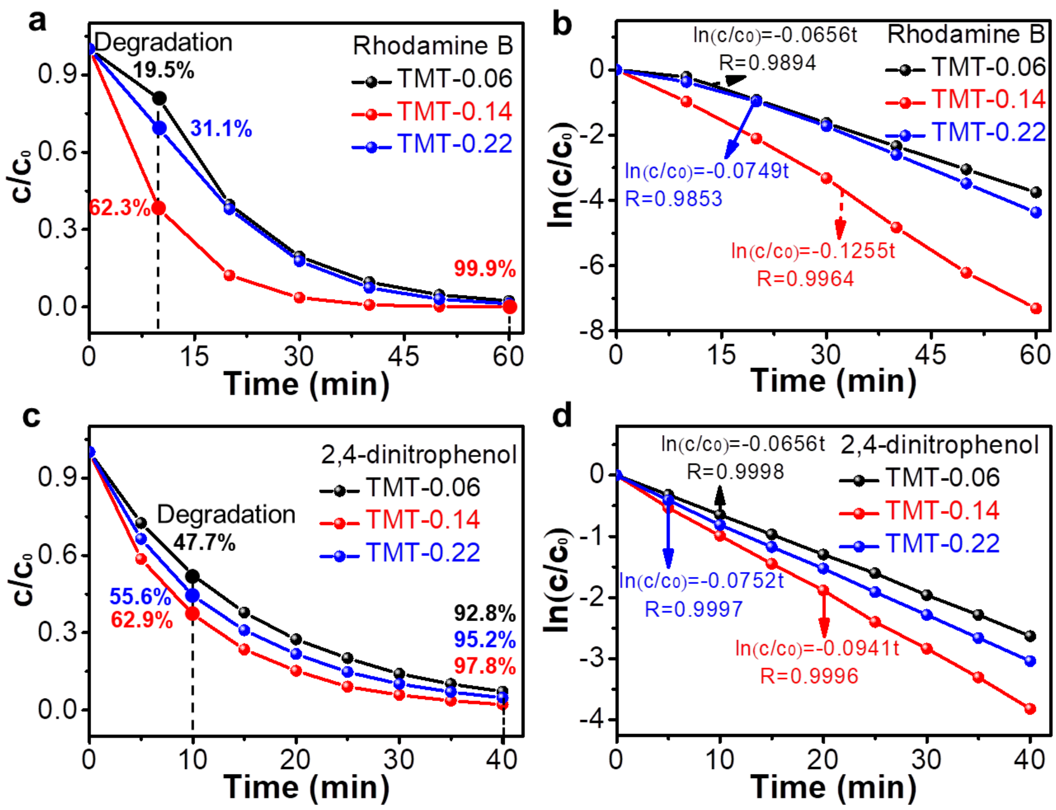

Fig. 3. Photocatalytic performance of TMT-0.06, TMT-0.14, and TMT-0.22. (a) Photocatalytic efficiencies and (b) pseudo-first-order kinetics plots for rhodamine B in the presence of 15 mg/L rhodamine B under solar-simulated light irradiation. (c) Photocatalytic efficiencies and (d) pseudo-first-order kinetics plots for 2,4-dinitrophenol in the presence of 150 mg/L 2,4-dinitrophenol under solar-simulated light irradiation.

The effect of the photocatalytic degradation time on the UV-vis absorption spectrum of residual rhodamine B and 2,4-dinitrophenol was also studied and depicted in **Fig. 4**. The concentration of rhodamine B and 2,4-dinitrophenol was 15 mg/L while the quantity of TMT-0.14 was 0.1 g/L. As can be seen**,** the characteristic absorbance peaks of rhodamine B and 2,4-dinitrophenol decrease with time and finally vanish after 60 minutes, suggesting that the majority of rhodamine B and 2,4-dinitrophenol are degraded into CO_2, H_2O, and others. To illustrate the photocatalytic performance of the materials studied in this work, the comparison of the degradation rates of TMT-0.14 in this work and other reports is shown in **Fig. 4**c.

Obviously, the degradation rate of TMT-0.14 prepared herein is superior to most of the TiO_2 nanotube array composites [34] and TiO_2 nanotube composites [35-38] reported in the literatures.

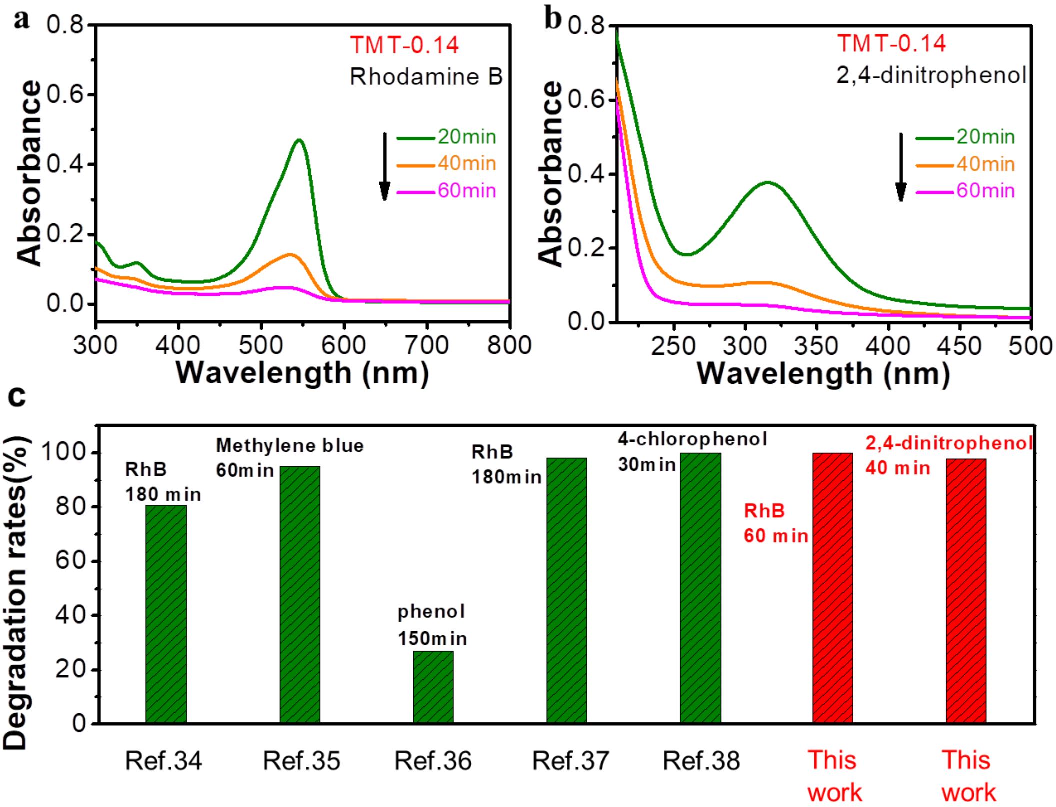

Fig. 4. Effect of photocatalytic degradation time of 0.1 g/L TMT-0.14 sample on UV-vis absorption spectrum of (a) rhodamine B and (b) 2,4-dinitrophenol under the simulated solar light irradiation. (c) Comparison of the degradation rates of TMT-0.14 in this work and other reports.

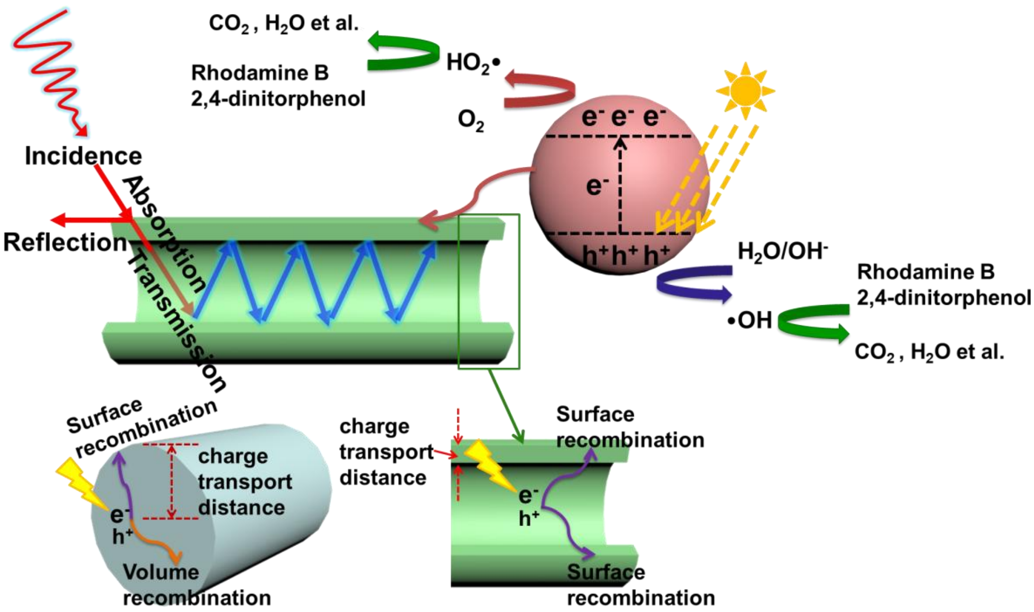

Fig. 5. Schematic diagram of light scattering phenomenon and photogenerated electrons and holes transfer in TiO_2 microtubes.

According to the results discussed above, a photocatalytic mechanism for the charge separation and transfer of TiO_2 microtubes with tunable thickness is proposed and illustrated in **Fig. 5**. TiO_2 microtubes with tunable thickness possess many significant advantages, such as multiple scattering for light harvesting and the reduction of the transport distance of photogenerated carriers to decrease the recombination of carriers [33]. There are a lot of void spaces in the hollow structure, which are easy to produce light-trapping effect [33]. After light penetrates into the wall of TiO_2 microtubes, the incident light is scattered multiple times within the microtubes as shown in **Fig. 5**. The microtube has secondary absorption of the scattered light to enhance the light-harvesting and improve the utilization of the incident light. This behavior is similar to the report in multiple shell CeO_2 hollow microspheres [30]. Compared with fibers, the tubular structure significantly reduces the charge-transport distance, inhibits the recombination of carriers in the volume, and significantly improves the charge separation efficiency [17]. When TiO_2 absorbs incident light of a certain energy, the valence band electrons are transferred to the conduction band, forming free-moving photogenerated electrons and producing abundant holes [39]. The photogenerated holes move to the surface of the TiO_2 microtubes and promote the activation of H_2O and OH^-, subsequently generating •OH [40]. Simultaneously, photogenerated electrons transferred to the surface of the photocatalyst can react with O_2 and form HO_2•. The species HO_2• and •OH (with high oxidation capability) can directly oxidize rhodamine B and 2,4-dinitrophenol into CO_2, H_2O, and other products [41].

4. Conclusion

One-step electrospinning followed by a calcination process has been developed to synthesize TiO_2 microtubes with controlled wall thicknesses by altering the dosage of liquid paraffin. Analyses of UV-vis diffuse reflectance spectra, photoluminescence emission spectra, and photocurrent density measurements show that an appropriate wall thickness can favor light harvesting, photocurrent density, and separation efficiency of charge root in the light scattering effect. Photocatalytic performance of TiO_2 microtubes with distinct wall thicknesses were compared by the degradation of rhodamine B and 2,4-dinitrophenol under simulated solar-light irradiation. The results show that TMT-0.14 exhibits the best photocatalytic performance, and the degradation rates of rhodamine B and 2,4-dinitrophenol by TiO_2 microtubes are 99.9 % within 60 minutes and 97.8 % within 40 minutes, respectively, which is attributed to the TiO_2 microtubes with suitable wall thickness can balance light-harvesting capability and charge separation efficiency while facilitating a large specific surface area. Our study provides a new strategy to adjust the wall thickness of TiO_2 microtubes and new approach to enhance the photocatalytic performance of TiO_2.

Author contributions

All authors have given approval to the final version of the manuscript.

Competing interests

The authors declare no competing financial interests.

Acknowledgments

The authors acknowledge financial support from the National Natural Science Foundation of China (Grant Nos.: 51464020, 51704188, 51802181, 61705125 and 51702199), Jiangxi Natural Science Foundation (Grant Nos.: 20161BAB206164 and 20161BBH80062), and Austrlian Research Council.

References

[1] H.-J. Chen, Y.-L. Yang, M. Hong, J.-G. Chen, G.-Q. Suo, X.-J. Hou, L. Feng, Z.-G. Chen, Separable and recyclable meso-carbon@TiO_2/carbon fiber composites for visible-light photocatalysis and photoelectrocatalysis, Sustain. Mater. Technol. 21 (2019) e00105.

[2] S. Sakthivel, B. Neppolian, M.V. Shankar, B. Arabindoo, M. Palanichamy, V. Murugesan, Solar

photocatalytic degradation of azo dye: comparison of photocatalytic efficiency of ZnO and TiO_2, Sol. Energ. Mat. Sol. C. 77 (1) (2003) 65-82.

[3] J.-S. Hu, L.-L. Ren, Y.-G. Guo, H.-P. Liang, C.-L.-B. Dr, Mass production and high photocatalytic activity of ZnS nanoporous nanoparticles, Angew. Chem. 44 (8) (2005) 1269-1273.

[4] W. Zhao, B. Zhipeng, R. Ailing, G. Bin, W. Can, Sunlight photocatalytic activity of CdS modified TiO_2 loaded on activated carbon fibers, Appl. Surf. Sci. 256 (11) (2010) 3493-3498.

[5] S. Chen, L. Zeng, H. Tian, X. Li, J. Gong, Enhanced lattice oxygen reactivity over Ni-modified WO_3-based redox catalysts for chemical looping partial oxidation of methane, ACS Catal. 7 (5) (2017) 3548-3559.

[6] X. Li, C. Guan, Y. Hu, J. Wang, Nanoflakes of Ni-Co LDH and Bi_2O_3 assembled in 3D carbon fiber network for high-performance aqueous rechargeable Ni/Bi battery, ACS Appl. Mater. Inter. 9 (31) (2017) 26008-26015.

[7] M. Zhou, J. Yu, S. Liu, P. Zhai, L. Jiang, Effects of calcination temperatures on photocatalytic activity of SnO_2/TiO_2 composite films prepared by an EPD method, J. Hazard. Mater. 154 (1) (2008) 1141-1148.

[8] J. Wen, J. Xie, H. Zhang, A. Zhang, X. Li, Constructing multifunctional metallic Ni interface layers in the g-C_3N_4 nanosheets/amorphous NiS heterojunctions for efficient photocatalytic H_2 generation, ACS Appl. Mater. Inter. 9 (16) (2017) 14042.

[9] N.-C. Meng, J. Bo, W.-K.-C. Christopher, S. Chris, Recent developments in photocatalytic water treatment technology: a review, Water Res. 44 (10) (2010) 2997-3027.

[10] S. Chen, Y. Li, C. Wang, C. Wang, Visible-light-driven photocatalytic H_2 evolution from aqueous suspensions of perylene diimide dye-sensitized Pt/TiO_2 catalysts, RSC Adv. 5 (21) (2015) 15880-15885.

[11] A. Fujishima, K. Honda, Electrochemical photolysis of water at a semiconductor electrode, Nature 238 (5358) (1972) 37-38.

[12] G. Tian, Y. Chen, W. Zhou, K. Pan, C. Tian, X.-R. Huang, H. Fu, 3D hierarchical flower-like TiO_2 nanostructure: morphology control and its photocatalytic property, Crystengcomm 13 (8) (2011) 2994-3000.

[13] M. Anas, S.-H. Dong, K. Mahmoud, H. Park, Abdel-Wahab. A, Photocatalytic degradation of organic dye using titanium dioxide modified with metal and non-metal deposition, Mat. Sci. Semicon. Proc. 41 (2015) 209-218.

[14] W. Hua, Q. Xie, H.-T. Y, C. Shuo, Fabrication of a TiO_2/carbon nanowall heterojunction and its photocatalytic ability, Carbon 46 (8) (2008) 1126-1132.

[15] C.-A. Linkous, G.-J. Carter, D.-B. Locuson, A.-J. Ouellette, L.-A. Smitha, Photocatalytic inhibition of algae growth using TiO_2, WO_3, and cocatalyst modifications, Environ. Sci. Technol. 34 (22) (2000) 4754-4758.

[16] A.-L. Costa, S. Ortelli, M. Blosi, S. Albonetti, A. Vaccari, M. Dondi, TiO_2 based photocatalytic coatings: from nanostructure to functional properties, Chem. Eng. J. 225 (225) (2013) 880-886.

[17] P. Zhang, T. Wang, X. Chang, J. Gong, Effective charge carrier utilization in photocatalytic conversions, Accounts Chem. Res. 49 (5) (2016) 911-921.

[18] M. Xiao, Z. Wang, M. Lyu, B. Luo, S. Wang, G. Liu, H.-M. Cheng, L. Wang, Hollow nanostructures for photocatalysis: advantages and challenges, Adv. Mater. 31 (38) (2019) e1801369.

[19] S. Ding, J.-S. Chen, Z. Wang, Y.-L. Cheah, S. Madhavi, X. Hu, X.-W. Lou, TiO_2 hollow spheres with large amount of exposed (001) facets for fast reversible lithium storage, J. Mater. Chem. 21 (6) (2011) 1677-1680.

[20] M. Alexander, K. Pandian, Linen fiber template-assisted preparation of TiO_2 nanotubes: palladium nanoparticle coating and electrochemical applications, J. Solid State Electr. 17 (4) (2013) 1117-1125.

[21] M.-Z. Ge, Q.-S. Li, C.-Y. Cao, J.-Y. Huang, Y.-K. Lai, One-dimensional TiO_2 nanotube photocatalysts for solar water splitting, Adv. Sci. 4 (1) (2016) 1600152.

[22] Q. Zhao, Q. Wang, Z. Liu, L. Qiu, X. Tian, S. Zhang, S. Gao, Fabrication and photoelectrochemical performance of Ag/AgBr sensitized TiO_2 nanotube arrays for environmental and energy applications, Sep. Purif. Technol. 209 (2019) 782-788.

[23] D. Wang, T. Hisatomi, T. Takata, C. Pan, M. Katayama, J. Kubota, K. Domen, Core/Shell photocatalyst with spatially separated co-catalysts for efficient reduction and oxidation of water, Angew. Chem. 52 (43) (2013) 11252-11256.

[24] Z. Liu, Q. Wang, X. Tan, Y. Wang, R. Jin, S. Gao, Enhanced photocatalytic performance of TiO_2 NTs decorated with chrysanthemum-like BiOI nanoflowers, Sep. Purif. Technol. 215 (2019) 565-572.

[25] Z. Liu, Y. Song, Q. Wang, Y. Jia, X. Tan, X. Du, S. Gao, Solvothermal fabrication and construction of highly photoelectrocatalytic TiO_2 NTs/Bi_2MoO_6 heterojunction based on titanium mesh, J. Colloid Interf. Sci. 556 (2019) 92-101.

[26] L. Qiu, Q. Wang, Z. Liu, Q. Zhao, X. Tian, H. Li, S. Gao, Preparation of 3D TiO_2 nanotube arrays photoelectrode on Ti mesh for photoelectric conversion and photoelectrocatalytic removal of pollutant, Sep. Purif. Technol. 207 (2018) 206-212.

[27] Z. Su, W. Zhou, Formation, morphology control and applications of anodic TiO_2 nanotube arrays, J. Mater. Chem. 21 (25) (2011) 8955-8950.

[28] Y.-L. Yang, H.-J. Chen, X. Zou, X.-L. Shi, W.-D. Liu, L. Feng, G. Suo, X. Hou, X. Ye, L. Zhang, C. Sun, H. Li, C. Wang, Z.-G. Chen, Flexible carbon-fiber/semimetal Bi nanosheet arrays as separable and recyclable plasmonic photocatalysts and photoelectrocatalysts, ACS Appl. Mater. Inter. 12 (22) (2020) 24845-24854.

[29] T. Wang, J. Wei, H. Shi, M. Zhou, Y. Zhang, Q. Chen, Z. Zhang, Preparation of electrospun Ag/TiO_2 nanotubes with enhanced photocatalytic activity based on water/oil phase separation, Physica E. 86 (2017) 103-110.

[30] J. Qi, K. Zhao, G. Li, Y. Gao, H. Zhao, R. Yu, Z. Tang, Multi-shelled CeO_2 hollow microspheres as superior photocatalysts for water oxidation, Nanoscale 6 (8) (2014) 4072-4077.

[31] L. Li, A.-S. Paul, S.-R. Gregory, Photocatalysts with internal electric fields, Nanoscale 6 (1) (2014) 24-42.

[32] D.-V. Bavykin, V.-N. Parmon, A.-A. Lapkin, F.-C. Walsh, The effect of hydrothermal conditions on the mesoporous structure of TiO_2 nanotubes, J. Mater. Chem. 14 (22) (2004) 3370-3377.

[33] G. Prieto, H. Tuysuz, N. Duyckaerts, J. Knossalla, G.-H. Wang, F. Schuth, Hollow nano- and microstructures as catalysts, Chem. Rev. 116 (22) (2016) 14056-14119.

[34] Q. Wang, H. Li, X. Yu, Y. Jia, Y. Chang, S. Gao, Morphology regulated Bi_2WO_6 nanoparticles on TiO_2 nanotubes by solvothermal Sb^{3+} doping as effective photocatalysts for wastewater treatment, Electrochim. Acta 330 (2020) 135167.

[35] U. Alam, M. Fleisch, I. Kretschmer, D. Bahnemann, M. Muneer, One-step hydrothermal synthesis of Bi-TiO_2 nanotube/graphene composites: an efficient photocatalyst for spectacular degradation of organic pollutants under visible light irradiation, Appl. Catal. B-Environ. 218 (2017) 758-769.

[36] H. Wang, Y. Liang, L. Liu, J. Hu, W. Cui, Highly ordered TiO_2 nanotube arrays wrapped with g-C_3N_4 nanoparticles for efficient charge separation and increased photoelectrocatalytic degradation of phenol, J. Hazard. Mater. 344 (2018) 369-380.

[37] J. Bi, X. Huang, J. Wang, T. Wang, H. Wu, J. Yang, H. Lu, H. Hao, Oil-phase cyclic magnetic adsorption to synthesize Fe_3O_4@C@TiO_2-nanotube composites for simultaneous removal of Pb(II) and Rhodamine B, Chem. Eng. J. 366 (2019) 50-61.

[38] J. Lim, Y. Yang, M.-R. Hoffmann, Activation of peroxymonosulfate by oxygen vacancies-enriched cobalt-doped black TiO_2 nanotubes for the removal of organic pollutants, Environ. Sci. Technol. 53 (12) (2019) 6972-6980.

[39] H.-Z. Zhang, J.-F. Banfield, Structural characteristics and mechanical and thermodynamic properties of nanocrystalline TiO_2, Chem. Rev. 114 (19) (2014) 9613-9644.

[40] Z. Zhang, F. Yu, L. Huang, J. Jiatieli, Y. Li, L. Song, Y. Ning, D.D. Dionysiou, Confirmation of hydroxyl radicals (·OH) generated in the presence of TiO_2 supported on AC under microwave irradiation, J. Hazard. Mater. 278 (2014) 152-157.

[41] C. Bahrini, A. Parker, C. Schoemaecker, C. Fittschen, Direct detection of HO_2 radicals in the vicinity of TiO_2 photocatalytic surfaces using cw-CRDS, Appl. Catal. B-Environ. 99 (3) (2010) 413-419.

The captions of Figures and Tables

Fig. 1. SEM and TEM images of (a, d, g) TMT-0.06, (b, e, h) TMT-0.14, (c, f, i) TMT-0.22. (j) XRD patterns of TMT-0.06, TMT-0.14, and TMT-0.22. (k) Schematic diagram of synthesizing process using electrospinning and the effect of the dosage of liquid paraffin on the wall thickness of TiO_2 microtubes.

Fig. 2. UV-vis diffuse reflectance spectra, photoluminescence spectra, and photocurrent of TiO_2 microtubes of TMT-0.06, TMT-0.14, and TMT-0.22. (a) UV-vis diffuse reflectance spectra. (b) Optical band gap energy of TMT-0.06 TMT-0.14, and TMT-0.22. (c) Photoluminescence emission spectra excited under 320 nm UV light. (d) The photocurrent of TiO_2 microtubes with tunable wall thickness under the irradiation of solar-simulated light, Pt-wire is counter electrode, constant bias vs. SCE is 0.1 V, and the working electrode is 3.5 cm×1.0 cm in size.

Fig. 3. Photocatalytic performance of TMT-0.06, TMT-0.14, and TMT-0.22. (a) Photocatalytic efficiencies and (b) pseudo-first-order kinetics plots for rhodamine B in the presence of 15 mg/L rhodamine B under solar-simulated light irradiation. (c) Photocatalytic efficiencies and (d) pseudo-first-order kinetics plots for 2,4-dinitrophenol in the presence of 150 mg/L 2,4-dinitrophenol under solar-simulated light irradiation.

Fig. 4. Effect of photocatalytic degradation time of 0.1 g/L TMT-0.14 sample on UV-vis absorption spectrum of (a) rhodamine B and (b) 2,4-dinitrophenol under the simulated solar light irradiation. (c) Comparison of the degradation rates of TMT-0.14 in this work and other reports.

Fig. 5. Schematic diagram of light scattering phenomenon and photogenerated electrons and holes transfer in TiO_2 microtubes.

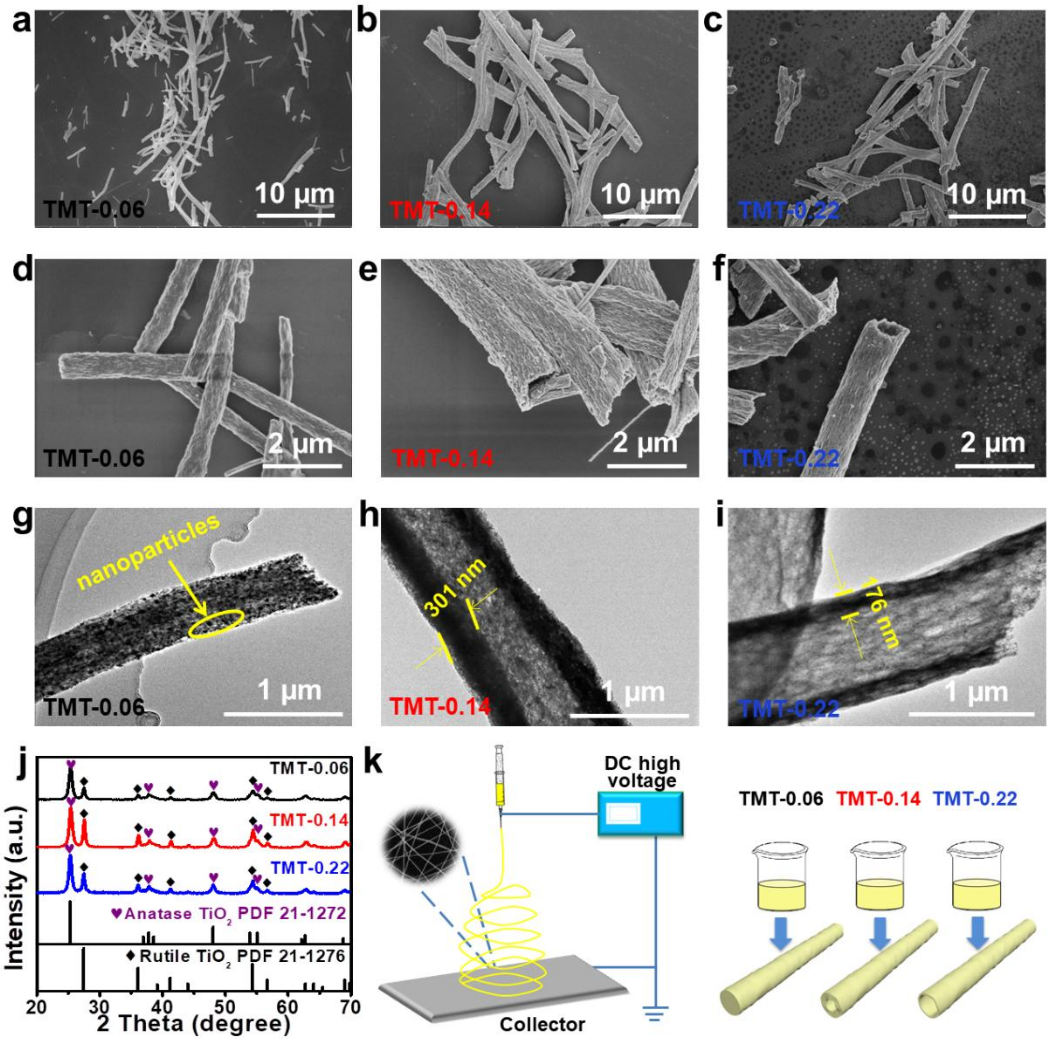
a
b
c
d
e
f
g
h
i
j
k
TMT-0.06
TMT-0.14
TMT-0.22
10 μm
2 μm
1 μm
nanoparticles
301 nm
176 nm
Intensity (a.u.)
2 Theta (degree)
Anatase TiO2 PDF 21-1272
Rutile TiO2 PDF 21-1276
DC high voltage
Collector

Fig. 1.

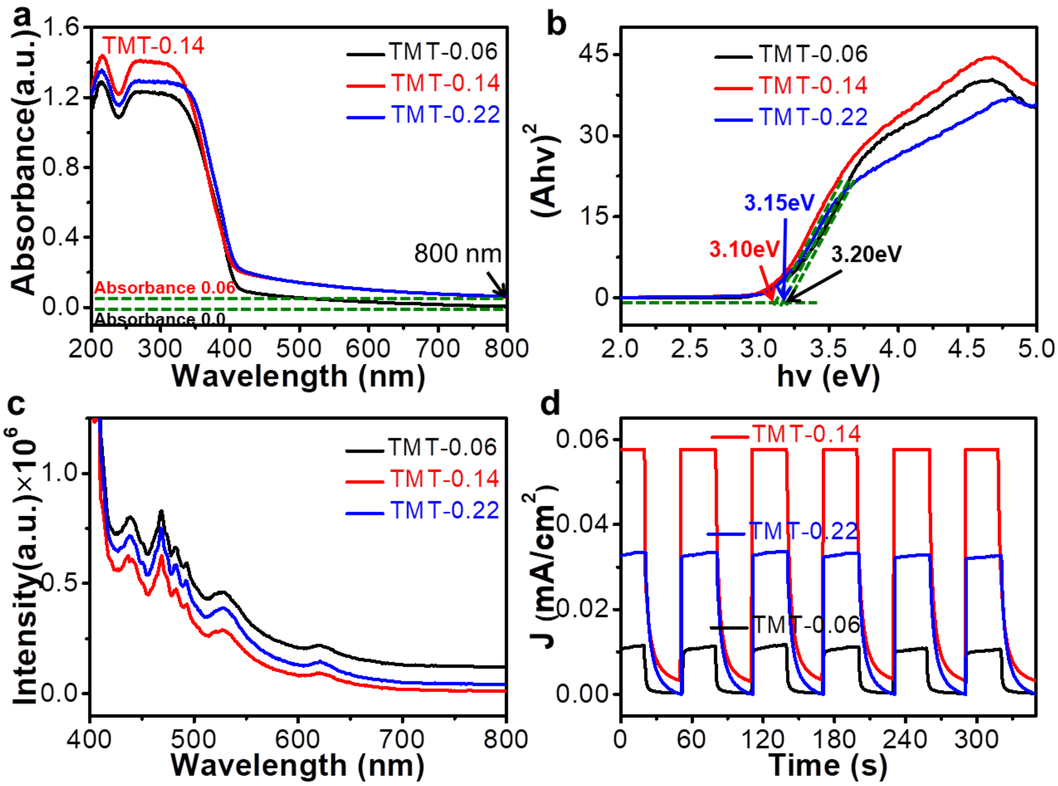

a
Absorbance(a.u.)
Wavelength (nm)
TMT-0.14
TMT-0.06
TMT-0.14
TMT-0.22
800 nm
Absorbance 0.06
Absorbance 0.0
b
(Ahv)^2
hv (eV)
TMT-0.06
TMT-0.14
TMT-0.22
3.15eV
3.10eV
3.20eV
c
Intensity(a.u.)×10^6
Wavelength (nm)
TMT-0.06
TMT-0.14
TMT-0.22
d
J (mA/cm^2)
Time (s)
TMT-0.14
TMT-0.22
TMT-0.06

Fig. 2.

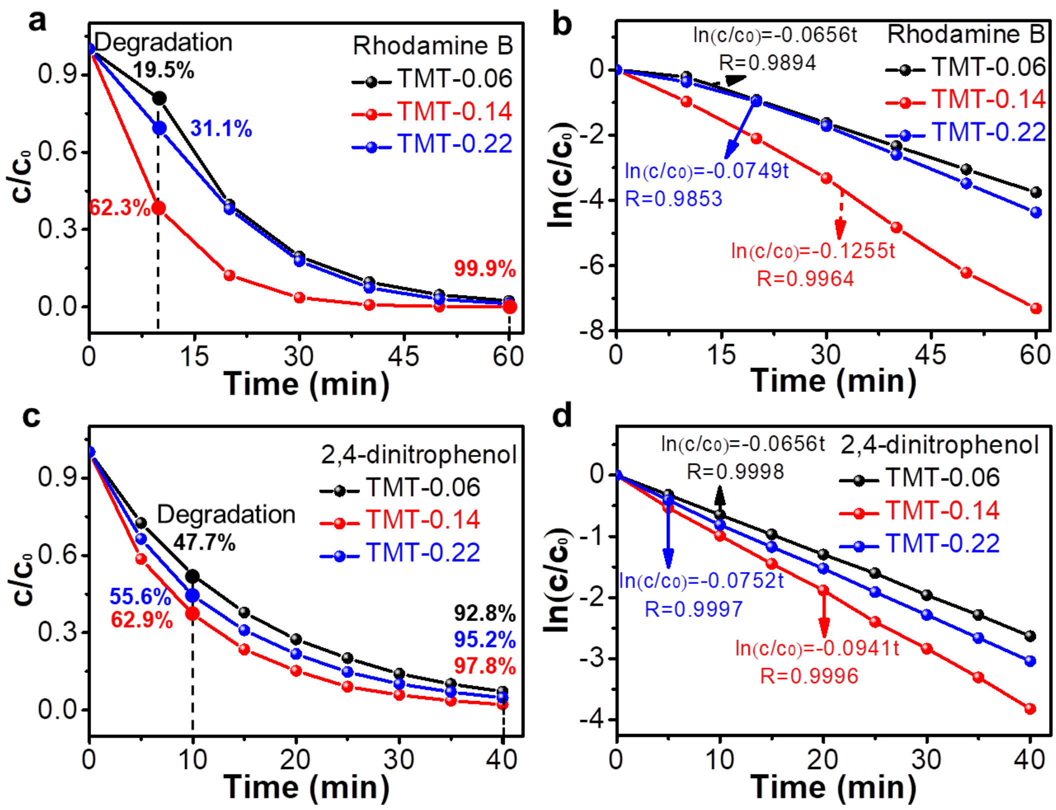
a
Degradation
19.5%
31.1%
62.3%
99.9%
Rhodamine B
TMT-0.06
TMT-0.14
TMT-0.22
c/c₀
Time (min)
b
ln(c/c0)=-0.0656t
R=0.9894
ln(c/c0)=-0.0749t
R=0.9853
ln(c/c0)=-0.1255t
R=0.9964
Rhodamine B
TMT-0.06
TMT-0.14
TMT-0.22
ln(c/c₀)
Time (min)
c
2,4-dinitrophenol
TMT-0.06
TMT-0.14
TMT-0.22
Degradation
47.7%
55.6%
62.9%
92.8%
95.2%
97.8%
c/c₀
Time (min)
d
ln(c/c0)=-0.0656t
R=0.9998
ln(c/c0)=-0.0752t
R=0.9997
ln(c/c0)=-0.0941t
R=0.9996
2,4-dinitrophenol
TMT-0.06
TMT-0.14
TMT-0.22
ln(c/c₀)
Time (min)

Fig. 3.

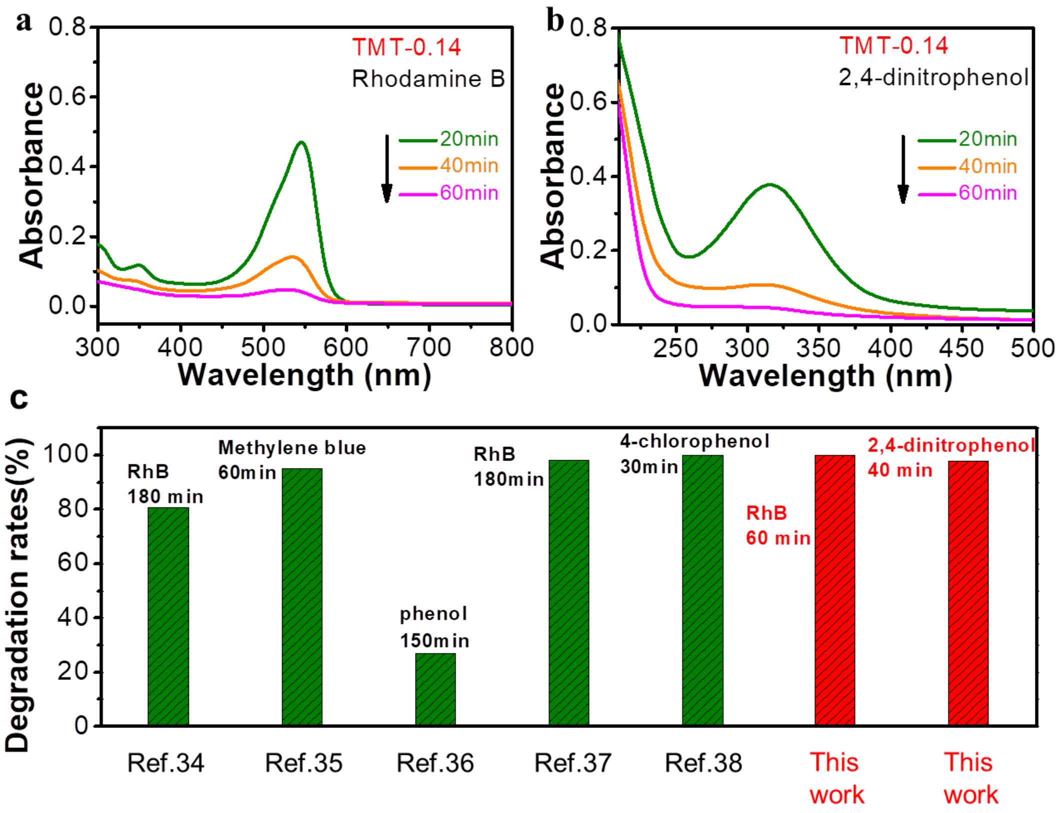
a
TMT-0.14
Rhodamine B
20min
40min
60min
Absorbance
Wavelength (nm)
b
TMT-0.14
2,4-dinitrophenol
20min
40min
60min
Absorbance
Wavelength (nm)
c
Degradation rates(%)
RhB
180 min
Methylene blue
60min
phenol
150min
RhB
180min
4-chlorophenol
30min
RhB
60 min
2,4-dinitrophenol
40 min
Ref.34
Ref.35
Ref.36
Ref.37
Ref.38
This work
This work

Fig. 4.

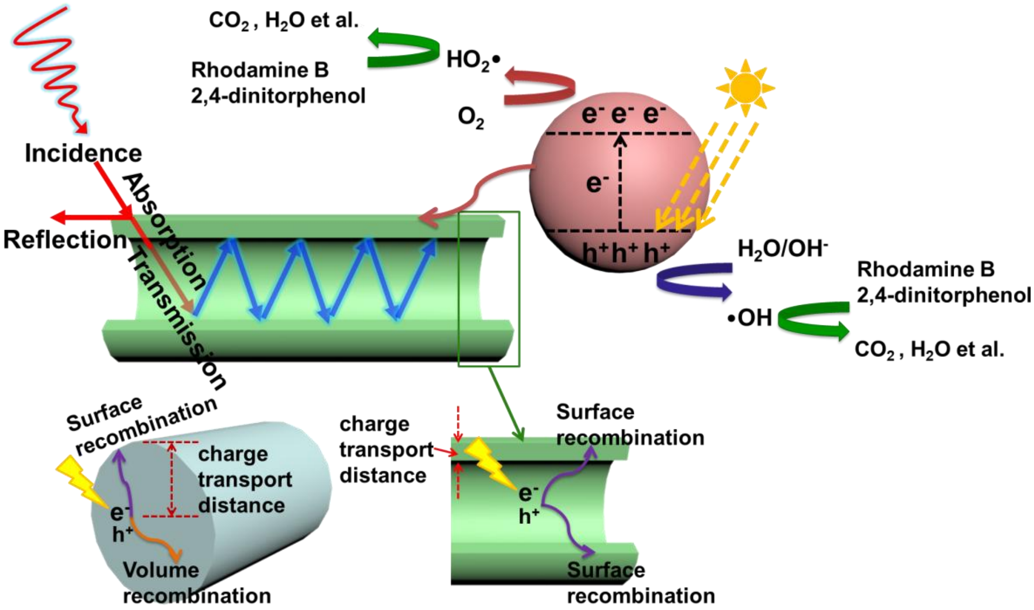

CO2 , H2O et al.
HO2•
Rhodamine B
2,4-dinitorphenol
O2
e- e- e-
e-
h+ h+ h+
H2O/OH-
Rhodamine B
2,4-dinitorphenol
•OH
CO2 , H2O et al.
Incidence
Reflection
Absorption
Transmission
Surface recombination
charge transport distance
e-
h+
Volume recombination
charge transport distance
Surface recombination
e-
h+
Surface recombination

Fig. 5.

Tuning wall thickness of TiO_2 microtubes for an enhanced photocatalytic activity with thickness-dependent charge separation efficiency

Xinxin Zou[1,a], *Yanling Yang*[1,a,*], *Huajun Chen*[1,2], *Xiao-Lei Shi*[3,4], *Guoquan Suo*[1], *Xiaohui Ye*[1], *Li Zhang*[1], *Xiaojiang Hou*[1], *Lei Feng*[1], *Zhi-Gang Chen*[3,4,*]

[1]School of Materials Science and Engineering, Shaanxi Key Laboratory of Green Preparation and Functionalization for Inorganic Materials, Shaanxi University of Science and Technology, Xi'an 710021, PR China

[2]Department of Environment and Chemistry, Luoyang Institute of Science and Technology, Luoyang 471023, PR China

[3]Centre for Future Materials, University of Southern Queensland, Springfield Central, QLD 4300, Australia.

[4]School of Mechanical and Mining Engineering, The University of Queensland, QLD 4072, Australia

[a] The first two authors contributed equally to this work

Corresponding Authors

* Yanling Yang: yangyanling@sust.edu.cn.

* Zhi-Gang Chen: zhigang.chen@usq.edu.au; zhigang.chen@uq.edu.au.

ABSTRACT

TiO_2 microtubes with tunable wall thickness have been synthesized by a one-step electrospinning method linked with a calcination process. The wall thickness of TiO_2 microtubes can be easily tuned by altering the dosage of liquid paraffin. The influence of the thickness on the light-harvesting ability and separation efficiency of the photogenerated carriers was studied using ultraviolet-visible (UV-vis) diffuse reflectance spectroscopy, photoluminescence emission spectroscopy, and photocurrent density measurements. Results show that TiO_2 microtubes with an appropriate thickness exhibit enhanced light scattering effect, UV-vis light-harvesting ability, charge separation efficiency, and photocatalytic performance. The degradation rates of rhodamine B and 2,4-dinitrophenol by using TiO_2 microtubes synthesized at a dosage of 0.14 g/mL liquid paraffin are 99.9 % within 60 minutes and 97.8 % within 40 minutes, respectively, which are higher than most of the reported values. All these results suggest that our work provides an ideal strategy for adjusting the wall thickness of TiO_2 microtubes and new approach to enhance the photocatalytic performance of TiO_2.

Keywords: Electrospinning, TiO_2, Microtube, Wall thickness, Thickness-dependent, Photocatalysis

1. Introduction

With ever-increasing human activities, environmental pollution has been considered as a common challenge. Over the last decades, extensive studies have concentrated on developing high-efficiency photocatalysts including TiO_2 [1], ZnO [2], ZnS [3], CdS [4], WO_3 [5], Bi_2O_3 [6], SnO_2 [7], and g-C_3N_4 [8], to degrade the organic contaminants in wastewater [9]. Due to the unique advantages of TiO_2, such as high chemical stability, nontoxicity, controllable structure/morphology, and economic effectiveness [10], TiO_2-based photocatalysts are among the most extensively investigated [11]. Nevertheless, its wide band gap (approximately 3.2 eV) limits the light absorption in the visible-light region and severely constrain its application of TiO_2. Furthermore, the lower separation efficiency of the photogenerated carriers adversely affects the photocatalytic activity of TiO_2.

To enhance the photocatalytic activity of TiO_2-based materials, several strategies including morphology control [12], metal or non-metal doping [13], heterojunction [14], and the use of cocatalysts [15], have been developed. Particularly, the microstructures of photocatalysts have a significant influence on their light-absorption ability and charge separation efficiency [16]. It has been reported that the hollow structures show multiple light scattering [17] and enhanced solar-energy conversion efficiency [18]. Therefore, the hollow structure of TiO_2 microtubes can shorten the migration distance of the photogenerated carriers, leading to a remarkable suppression of charge recombination [19]. In addition, the large specific surface area of TiO_2 microtubes provides plentiful reactive sites, which can be used to adsorb reactant molecules.

To date, TiO_2 nano/microtubes have been fabricated using template-assisted techniques [20], solvothermal method [21], hydrothermal method [21], and electrochemical anodic oxidation [22]. However, post-treatment of template-assisted techniques, such as high-temperature annealing or acid/alkali treatments, can easily destroy the microstructure of TiO_2 nano/microtubes [23]. The reaction time of the solvothermal and hydrothermal methods can significantly affect the morphology and wall thickness of nano/microtubes and the large-scale preparation induces non-uniform size [21]. Electrochemical anodic oxidation is commonly used to prepare nanotubes. Qiu, Liu, and Zhao et al. successfully prepared TiO_2 nanotube arrays using the electrochemical anodic oxidation technology [22,24-26]. However, the type and concentration of electrolyte, pH value and temperature significantly affect the morphology of nanotubes [27]. Therefore, achieving a controllable wall thickness of TiO_2 nano/microtubes is still challenging. Compared with the above methods, the electrospinning technique can easily control the microstructure of continuous nano/microtubes and offer advantages such as flexibility, cost-effectiveness, and polymer versatility [28]. However, adjusting the wall thickness of the prepared TiO_2 nano/microtubes by the electrospinning technique remains a challenge.

In this work, we realize the controlling of the wall thickness in TiO_2 microtubes using a one-step electrospinning technique by simply varying the dosage of liquid paraffin. The morphologies, light-harvesting abilities, separation efficiencies of photogenerated carriers, and photocatalytic activities along with the photocatalytic mechanism of TiO_2 microtubes with tunable wall thickness are investigated in detail. TiO_2 microtubes with tunable wall thickness can balance light-harvesting and efficiently utilize photogenerated charge carriers and possess improved light-harvesting ability and solar-energy conversion efficiency. An appropriate wall thickness can shorten the distance of charge-migration and benefit the separation of photogenerated carriers during the photocatalytic process, resulting in a superior photocatalytic degradation.

2. Experimental

2.1 Materials

Polyvinylpyrrolidone (PVP, Mw = 1300000), butyl titanate ($C_{16}H_{36}O_4Ti$), acetylacetone ($C_5H_8O_2$), anhydrous ethanol (C_2H_5OH), and liquid paraffin were purchased from Shanghai Macklin Biochemical Co., Ltd. All the reagents used to prepare TiO_2 microtubes are of analytic grade, without additional purification.

2.2 Fabrication of TiO_2 microtubes

TiO_2 microtubes were prepared using the electrospinning technique. First, PVP (1.2 g) was dissolved in 10 mL anhydrous ethanol under magnetic stirring. Then, anhydrous ethanol, acetylacetone, and butyl titanate were mixed with 1:1:1 mass ratio and then added into 5 mL PVP solution to obtain a clear solution. Finally, different dosages of liquid paraffin were added to the 5 mL mixed solution. After magnetic stirring for 48 h, viscous solutions were obtained.

The electrospinning apparatus comprises a high voltage power supply that generates an electric field of 0-30 kV, a syringe with an inner diameter of 0.6 mm at the capillary tip, and a micro-injection pump. A high voltage (18 KV) was employed, while the distance was 20 cm between the capillary tip and the aluminum foil collector. The solution was injected (using the micro-injection pump) at a constant rate of 0.3 mL/h and collected using aluminum foil. After electrospinning, layers of white fibers on the aluminum foil were collected and then calcined at 500 ℃ for 4 hours in air at a heating rate of 5 ℃/min. The obtained powder samples of TiO_2 microtubes were finally collected and treated with different dosages of liquid paraffin. The as-prepared TiO_2 microtubes using different liquid paraffin dosages were labeled as TMT-0.06, TMT-0.14, and TMT-0.22 (where TMT is the abbreviation for TiO_2 microtubes, and the subsequent digits show the dosage of liquid paraffin used; for instance, TMT-0.06 describes the TiO_2-microtube sample prepared by adding 0.06 g liquid paraffin to 1 mL mixed solution).

2.3 Characterization of photocatalysts

The morphology and structure of TiO_2 microtubes were studied using scanning electron microscopy (SEM, FEI Verios 460, USA), transmission electron microscopy (TEM, FEI Tecnai G2 F20 S-TWIN, USA), X-ray diffraction (Rigaku D/max2200Pc, Japan) using Cu-Kα radiation (λ = 1.5406 Å) with 2θ ranging from 20° to 70°, ultraviolet-visible (UV-vis) diffuse reflection spectroscopy (Agilent CARY 5000, USA) with an integrated sphere attachment ranging from 200 to 800 nm, and photoluminescence emission spectroscopy (F-7000, Hitachi, Japan).

Photoluminescence spectra were acquired using a fluorescence spectrophotometer (F-4500, Hitachi, Japan) at an excitation wavelength of 320 nm; the width of the slits for excitation and emission were both 5 nm. The photocurrents were obtained using an electrochemical analyzer (CHI 660D, China). Photocurrent measurements on the TiO_2 microtubes were performed on a CHI660E electrochemical workstation at room temperature using a standard three-electrode cell setup containing a platinum wire, saturated calomel electrode (SCE), and TiO_2 microtubes as the counter, reference, and working electrodes, respectively. Sodium sulfate solutions were used as electrolytes.

2.4 Photocatalytic experiment

The photocatalytic activity of TiO_2 microtubes was investigated by degrading organic solutions containing rhodamine B and 2, 4-dinitrophenol (15 mg/L) under simulated solar light (CDM-T 70W/942, Philips). First, 0.01 g samples were dispersed in 100 mL organic solution (15 mg/L) at a TiO_2-microtube concentration of 0.1 g/L. After ultrasonic dispersion for 10 minutes, the suspension was stirred 30 minutes in the dark to achieve the equilibrium of absorption-desorption among the photocatalyst and the organics. Afterwards, the blend containing the photocatalyst and organic solution was irradiated with simulated solar light. At certain time intervals, the mixture was centrifuged, and the residual organics were analyzed by UV-vis absorption spectroscopy.

During the photocatalytic process, the concentrations of rhodamine B and 2,4-dinitrophenol were periodically determined via spectrophotometry. The degradation rates of rhodamine B and 2,4-dinitrophenol were calculated using Eq. (1) : [1]

$$\textit{Degradation Rate} = \frac{c_0 - c_t}{c_0} \times 100\ \% \qquad (1)$$

where c_0 (mg/L) and c_t (mg/L) are the concentrations of rhodamine B and 2,4-dinitrophenol at time 0 and time *t*, respectively. The degradation rates of rhodamine B and 2, 4-dinitrophenol was described using a pseudo-first-order kinetics Eq. (2):

$$ln\frac{c_t}{c_0} = -k \times t \quad (2)$$

where *k* is the first-order kinetic rate constant of rhodamine B and 2,4-dinitrophenol during the photocatalytic process.

3. Results and discussion

Fig. 1a-c and **1d-f** show typical low/high magnification SEM images of the as-prepared TMT-0.06, TMT-0.14, and TMT-0.22, respectively. As can be seen, the microtubes are randomly distributed, and their diameter is at a level of ~1μm. The morphology of TMT-0.06 is fiber-like (**Fig. 1d**), while TMT-0.14 (**Fig. 1e**) and TMT-0.22 (**Fig. 1f**) are hollow tubulars, indicating that TiO_2 microtubes can be successfully prepared by adding liquid paraffin. Moreover, many wrinkles appear on the surface of TiO_2 microfibers or microtubes due to the volatilization of liquid paraffin. To confirm the hollow structure of TiO_2, the microstructure and wall thickness of TiO_2 microtubes were also estimated by using TEM and shown in **Fig. 1g-i**. At a dosage of 0.06 g/mL, the sample consists of nanoparticles and exhibits a well-defined porous structure (**Fig. 1g**). Upon increasing the amount of liquid paraffin to 0.14 and 0.22 g/mL, a hollow structural morphology of TiO_2 microtubes can be observed. Besides, the wall thickness of TiO_2 microtubes decreases with the addition of liquid paraffin. When the dosages of liquid paraffin are 0.14 and 0.22 g/mL, the wall thickness of TiO_2 microtubes can be measured to be ~300 and 180 nm, respectively (**Fig. 1h-i**). The dosage of liquid paraffin can affect the wall thickness of TiO_2 microtubes. At high liquid paraffin concentrations, the liquid paraffin on the fiber surface volatilizes in the presence of anhydrous ethanol, thus promoting the aggregation of PVP and butyl titanate on the fiber surface. The remaining liquid paraffin is slowly separated from the remaining solvent and accumulates inside the fiber during the drying process [29]. The decrease in wall thickness may be triggered by volatilization of more liquid paraffin at high temperatures during calcination. These SEM and TEM results show that the morphology of TiO_2 microtubes can be tuned by controlling the dosage of liquid paraffin, indicating that our synthesis strategy has high controllability of the wall thickness in TiO_2 microtubes. **Fig. 1j** presents the XRD patterns of TiO_2 microtubes synthesized at different dosages of liquid paraffin. As can be seen, all samples comprised mixed anatase (JCPDS card No. 21-1272) and rutile TiO_2 (JCPDS card No. 21-1276), indicating that anatase/rutile homojunctions are existed in the as-prepared TiO_2 microtubes. In order to illustrate the effect of the dosage of liquid paraffin on the wall thickness of TiO_2 microtubes, a sketch map of fabrication of TiO_2 microtubes is schematically shown in **Fig. 1k**, where the liquid paraffin acts as soft template for the controlling of the wall thickness in TiO_2 microtubes.

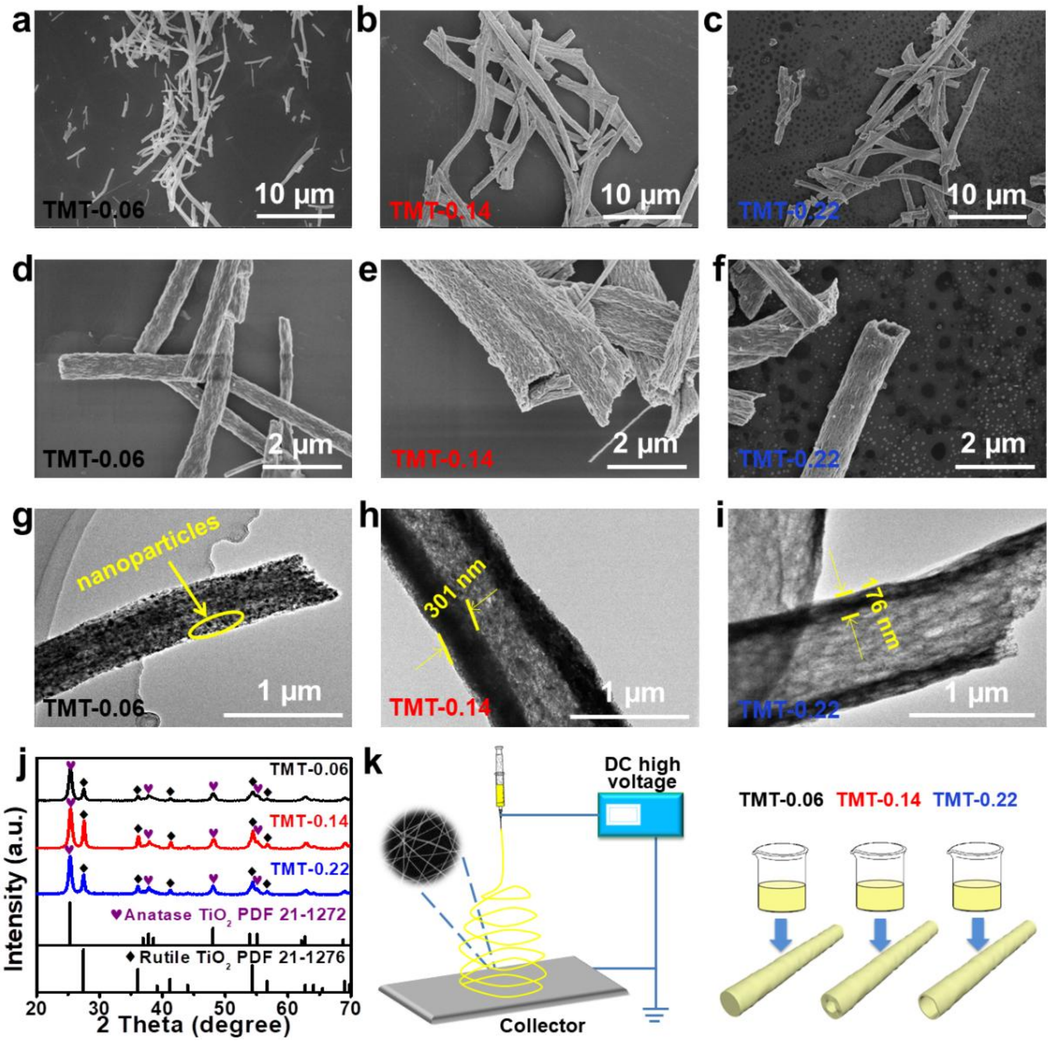

Fig. 1. SEM and TEM images of (a, d, g) TMT-0.06, (b, e, h) TMT-0.14, (c, f, i) TMT-0.22. (j) XRD patterns of TMT-0.06, TMT-0.14, and TMT-0.22. (k) Schematic diagram of synthesizing process using electrospinning and the effect of the dosage of liquid paraffin on the wall thickness of TiO_2 microtubes.

To evaluate the optical absorptivity of the as-prepared TMT-0.06, TMT-0.14, and TMT-0.22, a UV-vis diffuse reflectance spectroscopy was performed, and the results are shown in **Fig. 2a**. As can be seen, the optical absorptivity is increasing from TMT-0.06 to TMT-0.14 and then decreasing slightly for TMT-0.22, indicating that TMT-0.14 has a suitable wall thickness and the incident light can strongly scatter inside the microtubes of TMT-0.14, causing secondary absorption of the scattered light and increasing the optical absorptivity [30]. The microtube wall becomes thinner as the dosage of liquid paraffin continues to increase, and the hollow structure becomes more pronounced. Compared with TMT-0.14, TMT-0.22 shows a decreased optical absorptivity, suggesting that reducing the wall thickness increases the transmittance of the incident light, resulting in a weaker light scattering effect and thereby reducing light-harvesting activity [18].

Fig. 2b plots the optical band gap of the as-prepared TMT-0.06, TMT-0.14, and TMT-0.22 and shows that the optical band gaps of the TMT-0.06, TMT-0.14 and TMT-0.22 are 3.20, 3.10 and 3.15 eV, respectively. The measured band gap of all our samples is very close to that of anatase TiO_2 (3.2 eV). The slightly decreased band gap is caused by the distinct of hollow microstructures and the presence of rutile TiO_2 in the samples [29], indicating that a suitable hollow structure is conducive to reducing the band gap. **Fig. 2c** shows the photoluminescence emission spectra of the as-prepared TMT-0.06, TMT-0.14, and TMT-0.22 under ultraviolet excitation at 320 nm. TMT-0.14 exhibits a lower photoluminescence intensity compared to TMT-0.06, suggesting that the tubular structure of the microtubes can suppress the recombination of photogenerated carriers (excitation of TiO_2 under ultraviolet light). Actually, the tubular structure of the microtubes can largely shorten the migration distance of the photogenerated electrons and holes, and reduce the recombination of photogenerated carriers and improving the photocatalytic efficiency [19], However, excessive liquid paraffin addition (such as 0.22 g/mL) results in higher photoluminescence intensity of TMT-0.22 because the thin wall may reduce the charge-driving force and weaken the separation and transfer of charge, which is harmful to the suppression of photogenerated carrier recombination [31].

Fig. 2d shows the photocurrent response of the as-prepared TMT-0.06, TMT-0.14, and TMT-0.22 to the solar-simulated light irradiation of 0.1 M Na_2SO_4 electrolyte at the voltage of 0.1 V. With increasing the concentration of liquid paraffin, the photocurrent density of TMT-0.14 is greater than TMT-0.06 and the photocurrent density of TMT-0.22 decreases slightly. The results of the photocurrent measurements suggest that TMT-0.14 has a suitable wall thickness, which is favorable for an improved light-absorption capability and plays an important role in the generation of photocurrent. However, the thinner wall thickness of TMT-0.22 did not correspond to better photocurrent density. If the wall thickness is below the width of the space-charge layer, the band bending is reduced [18] and the electric driving force is decreased, which deteriorates the separation and transfer of photogenerated carriers [32].

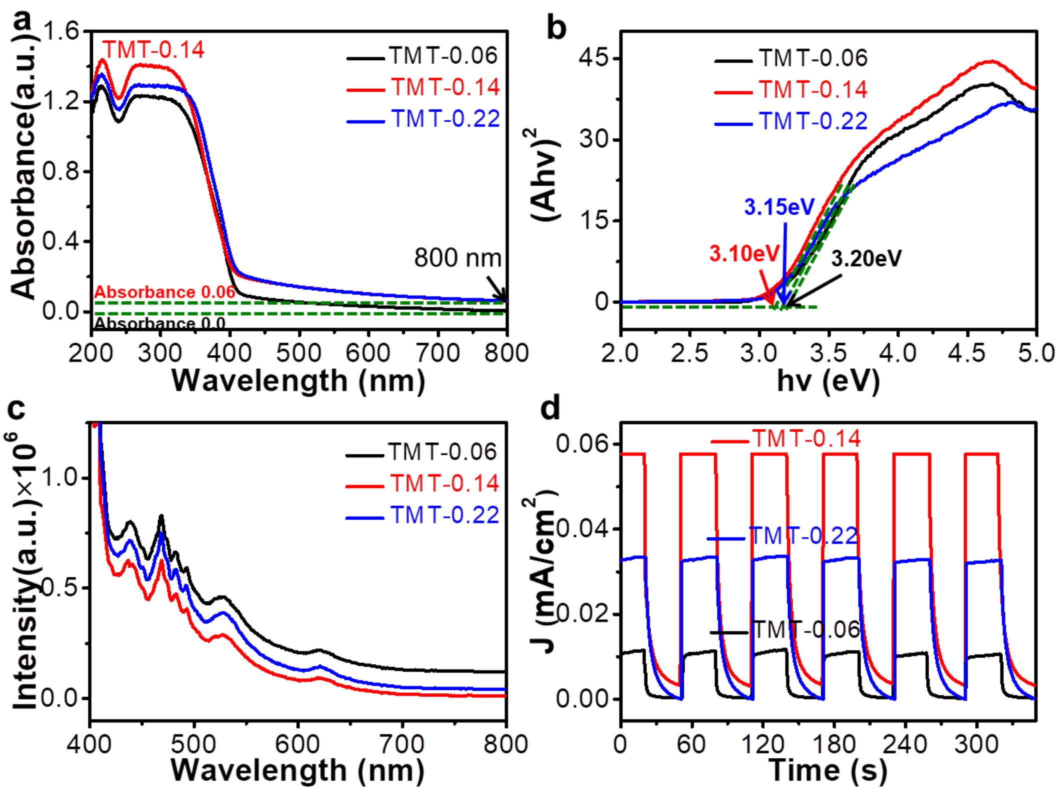

Fig. 2. UV-vis diffuse reflectance spectra, photoluminescence spectra, and photocurrent of TiO_2 microtubes of TMT-0.06, TMT-0.14, and TMT-0.22. (a) UV-vis diffuse reflectance spectra. (b) Optical band gap energy of TMT-0.06 TMT-0.14, and TMT-0.22. (c) Photoluminescence emission spectra excited under 320 nm UV light. (d) The photocurrent of TiO_2 microtubes with tunable wall thickness under the irradiation of solar-simulated light, Pt-wire is counter electrode, constant bias vs. SCE is 0.1 V, and the working electrode is 3.5 cm×1.0 cm in size.

The photocatalytic activities of as-prepared TiO_2 microtubes were further evaluated by the photocatalytic degradations of rhodamine B and 2,4-dinitrophenol under simulated solar-light irradiation. **Fig. 3** shows the degradation processes and kinetics for rhodamine B and 2,4-dinitrophenol using TMT-0.06, TMT-0.14, and TMT-0.22. **Fig. 3a** shows that the degradation rate of photocatalytic of TMT-0.14 is 99.9 % after 60 minutes. **Fig. 3b** plots the degradation kinetics of rhodamine B for TMT-0.06, TMT-0.14, and TMT-0.22 and shows first-order kinetics. **Fig. 3c** shows the degradation processes of 2,4-dinitrophenol by TMT-06, TMT-0.14, and TMT-0.22. After 40 minutes of simulated solar-light irradiation, the photocatalytic degradation rates of TMT-0.06, TMT-0.14, and TMT-0.22 are 92.8 %, 97.8 %, and 95.2 %, respectively. **Fig. 3d** shows the degradation kinetics of 2,4-dinitrophenol for TMT-0.06, TMT-0.14, and TMT-0.22, which are also consistent with first-order kinetics. These results show that the catalytic activity of TiO_2 microtubes with different wall thickness is different, which should be attributed to their effects on the charge separation efficiency, specific surface area [32], and light-harvesting capability [33].

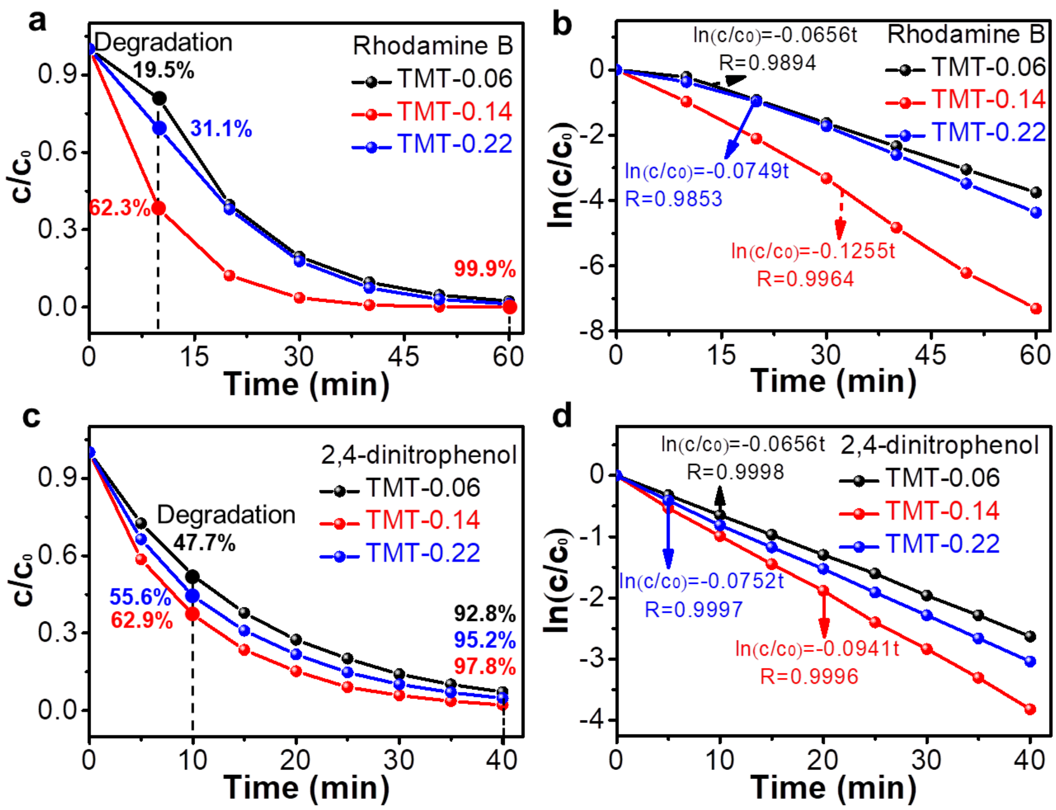

Fig. 3. Photocatalytic performance of TMT-0.06, TMT-0.14, and TMT-0.22. (a) Photocatalytic efficiencies and (b) pseudo-first-order kinetics plots for rhodamine B in the presence of 15 mg/L rhodamine B under solar-simulated light irradiation. (c) Photocatalytic efficiencies and (d) pseudo-first-order kinetics plots for 2,4-dinitrophenol in the presence of 150 mg/L 2,4-dinitrophenol under solar-simulated light irradiation.

The effect of the photocatalytic degradation time on the UV-vis absorption spectrum of residual rhodamine B and 2,4-dinitrophenol was also studied and depicted in **Fig. 4**. The concentration of rhodamine B and 2,4-dinitrophenol was 15 mg/L while the quantity of TMT-0.14 was 0.1 g/L. As can be seen**,** the characteristic absorbance peaks of rhodamine B and 2,4-dinitrophenol decrease with time and finally vanish after 60 minutes, suggesting that the majority of rhodamine B and 2,4-dinitrophenol are degraded into CO_2, H_2O, and others. To illustrate the photocatalytic performance of the materials studied in this work, the comparison of the degradation rates of TMT-0.14 in this work and other reports is shown in **Fig. 4c**.

Obviously, the degradation rate of TMT-0.14 prepared herein is superior to most of the TiO_2 nanotube array composites [34] and TiO_2 nanotube composites [35-38] reported in the literatures.

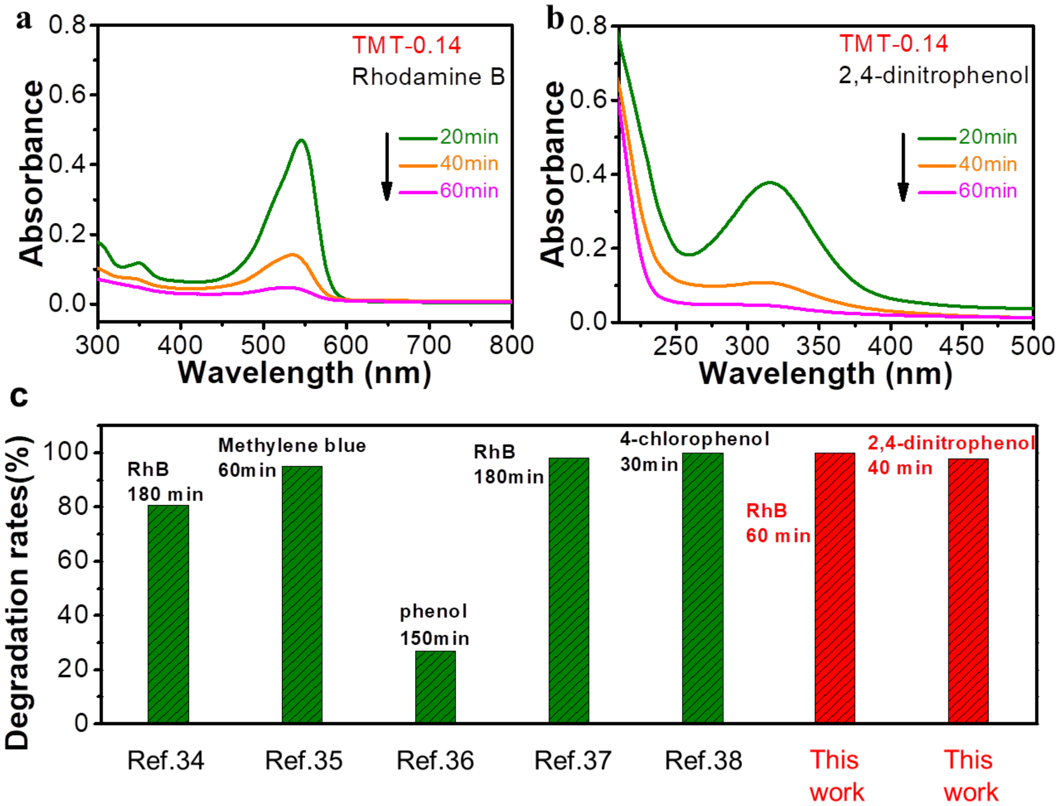

Fig. 4. Effect of photocatalytic degradation time of 0.1 g/L TMT-0.14 sample on UV-vis absorption spectrum of (a) rhodamine B and (b) 2,4-dinitrophenol under the simulated solar light irradiation. (c) Comparison of the degradation rates of TMT-0.14 in this work and other reports.

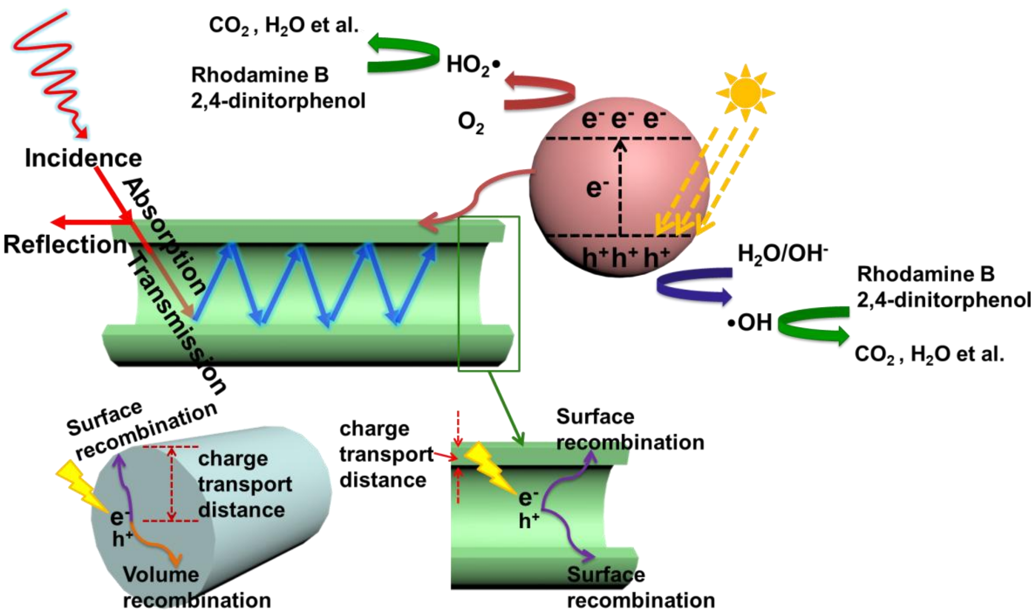

Fig. 5. Schematic diagram of light scattering phenomenon and photogenerated electrons and holes transfer in TiO_2 microtubes.

According to the results discussed above, a photocatalytic mechanism for the charge separation and transfer of TiO_2 microtubes with tunable thickness is proposed and illustrated in **Fig. 5**. TiO_2 microtubes with tunable thickness possess many significant advantages, such as multiple scattering for light harvesting and the reduction of the transport distance of photogenerated carriers to decrease the recombination of carriers [33]. There are a lot of void spaces in the hollow structure, which are easy to produce light-trapping effect [33]. After light penetrates into the wall of TiO_2 microtubes, the incident light is scattered multiple times within the microtubes as shown in **Fig. 5**. The microtube has secondary absorption of the scattered light to enhance the light-harvesting and improve the utilization of the incident light. This behavior is similar to the report in multiple shell CeO_2 hollow microspheres [30]. Compared with fibers, the tubular structure significantly reduces the charge-transport distance, inhibits the recombination of carriers in the volume, and significantly improves the charge separation efficiency [17]. When TiO_2 absorbs incident light of a certain energy, the valence band electrons are transferred to the conduction band, forming free-moving photogenerated electrons and producing abundant holes [39]. The photogenerated holes move to the surface of the TiO_2 microtubes and promote the activation of H_2O and OH^-, subsequently generating •OH [40]. Simultaneously, photogenerated electrons transferred to the surface of the photocatalyst can react with O_2 and form HO_2•. The species HO_2• and •OH (with high oxidation capability) can directly oxidize rhodamine B and 2,4-dinitrophenol into CO_2, H_2O, and other products [41].

4. Conclusion

One-step electrospinning followed by a calcination process has been developed to synthesize TiO_2 microtubes with controlled wall thicknesses by altering the dosage of liquid paraffin. Analyses of UV-vis diffuse reflectance spectra, photoluminescence emission spectra, and photocurrent density measurements show that an appropriate wall thickness can favor light harvesting, photocurrent density, and separation efficiency of charge root in the light scattering effect. Photocatalytic performance of TiO_2 microtubes with distinct wall thicknesses were compared by the degradation of rhodamine B and 2,4-dinitrophenol under simulated solar-light irradiation. The results show that TMT-0.14 exhibits the best photocatalytic performance, and the degradation rates of rhodamine B and 2,4-dinitrophenol by TiO_2 microtubes are 99.9 % within 60 minutes and 97.8 % within 40 minutes, respectively, which is attributed to the TiO_2 microtubes with suitable wall thickness can balance light-harvesting capability and charge separation efficiency while facilitating a large specific surface area. Our study provides a new strategy to adjust the wall thickness of TiO_2 microtubes and new approach to enhance the photocatalytic performance of TiO_2.

Author contributions

All authors have given approval to the final version of the manuscript.

Competing interests

The authors declare no competing financial interests.

Acknowledgments

The authors acknowledge financial support from the National Natural Science Foundation of China (Grant Nos.: 51464020, 51704188, 51802181, 61705125 and 51702199), Jiangxi Natural Science Foundation (Grant Nos.: 20161BAB206164 and 20161BBH80062), and Austrlian Research Council.

References

[1] H.-J. Chen, Y.-L. Yang, M. Hong, J.-G. Chen, G.-Q. Suo, X.-J. Hou, L. Feng, Z.-G. Chen, Separable and recyclable meso-carbon@TiO_2/carbon fiber composites for visible-light photocatalysis and photoelectrocatalysis, Sustain. Mater. Technol. 21 (2019) e00105.

[2] S. Sakthivel, B. Neppolian, M.V. Shankar, B. Arabindoo, M. Palanichamy, V. Murugesan, Solar

photocatalytic degradation of azo dye: comparison of photocatalytic efficiency of ZnO and TiO_2, Sol. Energ. Mat. Sol. C. 77 (1) (2003) 65-82.

[3] J.-S. Hu, L.-L. Ren, Y.-G. Guo, H.-P. Liang, C.-L.-B. Dr, Mass production and high photocatalytic activity of ZnS nanoporous nanoparticles, Angew. Chem. 44 (8) (2005) 1269-1273.

[4] W. Zhao, B. Zhipeng, R. Ailing, G. Bin, W. Can, Sunlight photocatalytic activity of CdS modified TiO_2 loaded on activated carbon fibers, Appl. Surf. Sci. 256 (11) (2010) 3493-3498.

[5] S. Chen, L. Zeng, H. Tian, X. Li, J. Gong, Enhanced lattice oxygen reactivity over Ni-modified WO_3-based redox catalysts for chemical looping partial oxidation of methane, ACS Catal. 7 (5) (2017) 3548-3559.

[6] X. Li, C. Guan, Y. Hu, J. Wang, Nanoflakes of Ni-Co LDH and Bi_2O_3 assembled in 3D carbon fiber network for high-performance aqueous rechargeable Ni/Bi battery, ACS Appl. Mater. Inter. 9 (31) (2017) 26008-26015.

[7] M. Zhou, J. Yu, S. Liu, P. Zhai, L. Jiang, Effects of calcination temperatures on photocatalytic activity of SnO_2/TiO_2 composite films prepared by an EPD method, J. Hazard. Mater. 154 (1) (2008) 1141-1148.

[8] J. Wen, J. Xie, H. Zhang, A. Zhang, X. Li, Constructing multifunctional metallic Ni interface layers in the g-C_3N_4 nanosheets/amorphous NiS heterojunctions for efficient photocatalytic H_2 generation, ACS Appl. Mater. Inter. 9 (16) (2017) 14042.

[9] N.-C. Meng, J. Bo, W.-K.-C. Christopher, S. Chris, Recent developments in photocatalytic water treatment technology: a review, Water Res. 44 (10) (2010) 2997-3027.

[10] S. Chen, Y. Li, C. Wang, C. Wang, Visible-light-driven photocatalytic H_2 evolution from aqueous suspensions of perylene diimide dye-sensitized Pt/TiO_2 catalysts, RSC Adv. 5 (21) (2015) 15880-15885.

[11] A. Fujishima, K. Honda, Electrochemical photolysis of water at a semiconductor electrode, Nature 238 (5358) (1972) 37-38.

[12] G. Tian, Y. Chen, W. Zhou, K. Pan, C. Tian, X.-R. Huang, H. Fu, 3D hierarchical flower-like TiO_2 nanostructure: morphology control and its photocatalytic property, Crystengcomm 13 (8) (2011) 2994-3000.

[13] M. Anas, S.-H. Dong, K. Mahmoud, H. Park, Abdel-Wahab. A, Photocatalytic degradation of organic dye using titanium dioxide modified with metal and non-metal deposition, Mat. Sci. Semicon. Proc. 41 (2015) 209-218.

[14] W. Hua, Q. Xie, H.-T. Y, C. Shuo, Fabrication of a TiO_2/carbon nanowall heterojunction and its photocatalytic ability, Carbon 46 (8) (2008) 1126-1132.

[15] C.-A. Linkous, G.-J. Carter, D.-B. Locuson, A.-J. Ouellette, L.-A. Smitha, Photocatalytic inhibition of algae growth using TiO_2, WO_3, and cocatalyst modifications, Environ. Sci. Technol. 34 (22) (2000) 4754-4758.

[16] A.-L. Costa, S. Ortelli, M. Blosi, S. Albonetti, A. Vaccari, M. Dondi, TiO_2 based photocatalytic coatings: from nanostructure to functional properties, Chem. Eng. J. 225 (225) (2013) 880-886.

[17] P. Zhang, T. Wang, X. Chang, J. Gong, Effective charge carrier utilization in photocatalytic conversions, Accounts Chem. Res. 49 (5) (2016) 911-921.

[18] M. Xiao, Z. Wang, M. Lyu, B. Luo, S. Wang, G. Liu, H.-M. Cheng, L. Wang, Hollow nanostructures for photocatalysis: advantages and challenges, Adv. Mater. 31 (38) (2019) e1801369.

[19] S. Ding, J.-S. Chen, Z. Wang, Y.-L. Cheah, S. Madhavi, X. Hu, X.-W. Lou, TiO_2 hollow spheres with large amount of exposed (001) facets for fast reversible lithium storage, J. Mater. Chem. 21 (6) (2011) 1677-1680.

[20] M. Alexander, K. Pandian, Linen fiber template-assisted preparation of TiO_2 nanotubes: palladium nanoparticle coating and electrochemical applications, J. Solid State Electr. 17 (4) (2013) 1117-1125.

[21] M.-Z. Ge, Q.-S. Li, C.-Y. Cao, J.-Y. Huang, Y.-K. Lai, One-dimensional TiO_2 nanotube photocatalysts for solar water splitting, Adv. Sci. 4 (1) (2016) 1600152.

[22] Q. Zhao, Q. Wang, Z. Liu, L. Qiu, X. Tian, S. Zhang, S. Gao, Fabrication and photoelectrochemical performance of Ag/AgBr sensitized TiO_2 nanotube arrays for environmental and energy applications, Sep. Purif. Technol. 209 (2019) 782-788.

[23] D. Wang, T. Hisatomi, T. Takata, C. Pan, M. Katayama, J. Kubota, K. Domen, Core/Shell photocatalyst with spatially separated co-catalysts for efficient reduction and oxidation of water, Angew. Chem. 52 (43) (2013) 11252-11256.

[24] Z. Liu, Q. Wang, X. Tan, Y. Wang, R. Jin, S. Gao, Enhanced photocatalytic performance of TiO_2 NTs decorated with chrysanthemum-like BiOI nanoflowers, Sep. Purif. Technol. 215 (2019) 565-572.

[25] Z. Liu, Y. Song, Q. Wang, Y. Jia, X. Tan, X. Du, S. Gao, Solvothermal fabrication and construction of highly photoelectrocatalytic TiO_2 NTs/Bi_2MoO_6 heterojunction based on titanium mesh, J. Colloid Interf. Sci. 556 (2019) 92-101.

[26] L. Qiu, Q. Wang, Z. Liu, Q. Zhao, X. Tian, H. Li, S. Gao, Preparation of 3D TiO_2 nanotube arrays photoelectrode on Ti mesh for photoelectric conversion and photoelectrocatalytic removal of pollutant, Sep. Purif. Technol. 207 (2018) 206-212.

[27] Z. Su, W. Zhou, Formation, morphology control and applications of anodic TiO_2 nanotube arrays, J. Mater. Chem. 21 (25) (2011) 8955-8950.

[28] Y.-L. Yang, H.-J. Chen, X. Zou, X.-L. Shi, W.-D. Liu, L. Feng, G. Suo, X. Hou, X. Ye, L. Zhang, C. Sun, H. Li, C. Wang, Z.-G. Chen, Flexible carbon-fiber/semimetal Bi nanosheet arrays as separable and recyclable plasmonic photocatalysts and photoelectrocatalysts, ACS Appl. Mater. Inter. 12 (22) (2020) 24845-24854.

[29] T. Wang, J. Wei, H. Shi, M. Zhou, Y. Zhang, Q. Chen, Z. Zhang, Preparation of electrospun Ag/TiO_2 nanotubes with enhanced photocatalytic activity based on water/oil phase separation, Physica E. 86 (2017) 103-110.

[30] J. Qi, K. Zhao, G. Li, Y. Gao, H. Zhao, R. Yu, Z. Tang, Multi-shelled CeO_2 hollow microspheres as superior photocatalysts for water oxidation, Nanoscale 6 (8) (2014) 4072-4077.

[31] L. Li, A.-S. Paul, S.-R. Gregory, Photocatalysts with internal electric fields, Nanoscale 6 (1) (2014) 24-42.

[32] D.-V. Bavykin, V.-N. Parmon, A.-A. Lapkin, F.-C. Walsh, The effect of hydrothermal conditions on the mesoporous structure of TiO_2 nanotubes, J. Mater. Chem. 14 (22) (2004) 3370-3377.

[33] G. Prieto, H. Tuysuz, N. Duyckaerts, J. Knossalla, G.-H. Wang, F. Schuth, Hollow nano- and microstructures as catalysts, Chem. Rev. 116 (22) (2016) 14056-14119.

[34] Q. Wang, H. Li, X. Yu, Y. Jia, Y. Chang, S. Gao, Morphology regulated Bi_2WO_6 nanoparticles on TiO_2 nanotubes by solvothermal Sb^{3+} doping as effective photocatalysts for wastewater treatment, Electrochim. Acta 330 (2020) 135167.

[35] U. Alam, M. Fleisch, I. Kretschmer, D. Bahnemann, M. Muneer, One-step hydrothermal synthesis of Bi-TiO_2 nanotube/graphene composites: an efficient photocatalyst for spectacular degradation of organic pollutants under visible light irradiation, Appl. Catal. B-Environ. 218 (2017) 758-769.

[36] H. Wang, Y. Liang, L. Liu, J. Hu, W. Cui, Highly ordered TiO_2 nanotube arrays wrapped with g-C_3N_4 nanoparticles for efficient charge separation and increased photoelectrocatalytic degradation of phenol, J. Hazard. Mater. 344 (2018) 369-380.

[37] J. Bi, X. Huang, J. Wang, T. Wang, H. Wu, J. Yang, H. Lu, H. Hao, Oil-phase cyclic magnetic adsorption to synthesize Fe_3O_4@C@TiO_2-nanotube composites for simultaneous removal of Pb(II) and Rhodamine B, Chem. Eng. J. 366 (2019) 50-61.

[38] J. Lim, Y. Yang, M.-R. Hoffmann, Activation of peroxymonosulfate by oxygen vacancies-enriched cobalt-doped black TiO_2 nanotubes for the removal of organic pollutants, Environ. Sci. Technol. 53 (12) (2019) 6972-6980.

[39] H.-Z. Zhang, J.-F. Banfield, Structural characteristics and mechanical and thermodynamic properties of nanocrystalline TiO_2, Chem. Rev. 114 (19) (2014) 9613-9644.

[40] Z. Zhang, F. Yu, L. Huang, J. Jiatieli, Y. Li, L. Song, Y. Ning, D.D. Dionysiou, Confirmation of hydroxyl radicals (·OH) generated in the presence of TiO_2 supported on AC under microwave irradiation, J. Hazard. Mater. 278 (2014) 152-157.

[41] C. Bahrini, A. Parker, C. Schoemaecker, C. Fittschen, Direct detection of HO_2 radicals in the vicinity of TiO_2 photocatalytic surfaces using cw-CRDS, Appl. Catal. B-Environ. 99 (3) (2010) 413-419.

The captions of Figures and Tables

Fig. 1. SEM and TEM images of (a, d, g) TMT-0.06, (b, e, h) TMT-0.14, (c, f, i) TMT-0.22. (j) XRD patterns of TMT-0.06, TMT-0.14, and TMT-0.22. (k) Schematic diagram of synthesizing process using electrospinning and the effect of the dosage of liquid paraffin on the wall thickness of TiO_2 microtubes.

Fig. 2. UV-vis diffuse reflectance spectra, photoluminescence spectra, and photocurrent of TiO_2 microtubes of TMT-0.06, TMT-0.14, and TMT-0.22. (a) UV-vis diffuse reflectance spectra. (b) Optical band gap energy of TMT-0.06 TMT-0.14, and TMT-0.22. (c) Photoluminescence emission spectra excited under 320 nm UV light. (d) The photocurrent of TiO_2 microtubes with tunable wall thickness under the irradiation of solar-simulated light, Pt-wire is counter electrode, constant bias vs. SCE is 0.1 V, and the working electrode is 3.5 cm×1.0 cm in size.

Fig. 3. Photocatalytic performance of TMT-0.06, TMT-0.14, and TMT-0.22. (a) Photocatalytic efficiencies and (b) pseudo-first-order kinetics plots for rhodamine B in the presence of 15 mg/L rhodamine B under solar-simulated light irradiation. (c) Photocatalytic efficiencies and (d) pseudo-first-order kinetics plots for 2,4-dinitrophenol in the presence of 150 mg/L 2,4-dinitrophenol under solar-simulated light irradiation.

Fig. 4. Effect of photocatalytic degradation time of 0.1 g/L TMT-0.14 sample on UV-vis absorption spectrum of (a) rhodamine B and (b) 2,4-dinitrophenol under the simulated solar light irradiation. (c) Comparison of the degradation rates of TMT-0.14 in this work and other reports.

Fig. 5. Schematic diagram of light scattering phenomenon and photogenerated electrons and holes transfer in TiO_2 microtubes.

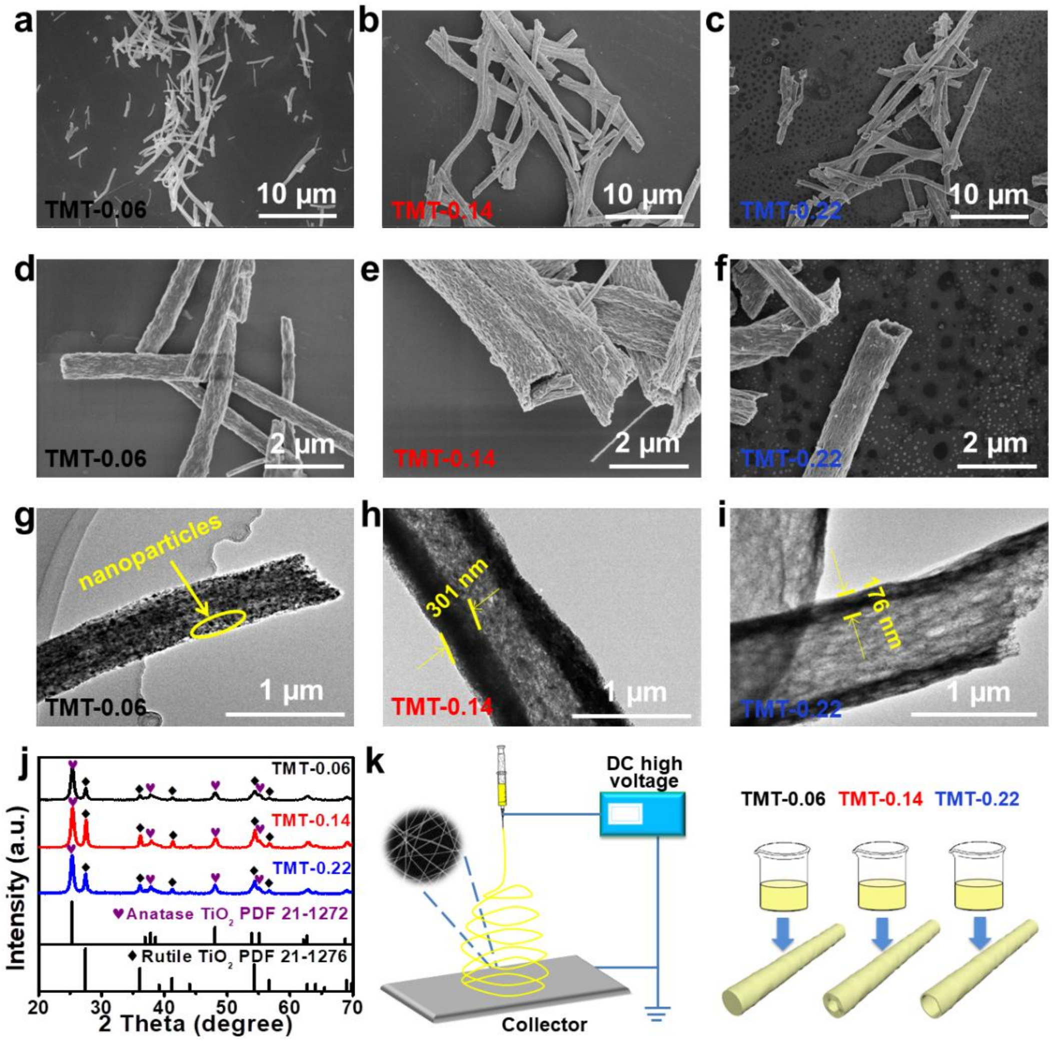

a
b
c
d
e
f
g
h
i
j
k
TMT-0.06
TMT-0.14
TMT-0.22
10 μm
2 μm
1 μm
nanoparticles
301 nm
176 nm
Intensity (a.u.)
2 Theta (degree)
♥Anatase TiO2 PDF 21-1272
♦Rutile TiO2 PDF 21-1276
DC high voltage
Collector

Fig. 1.

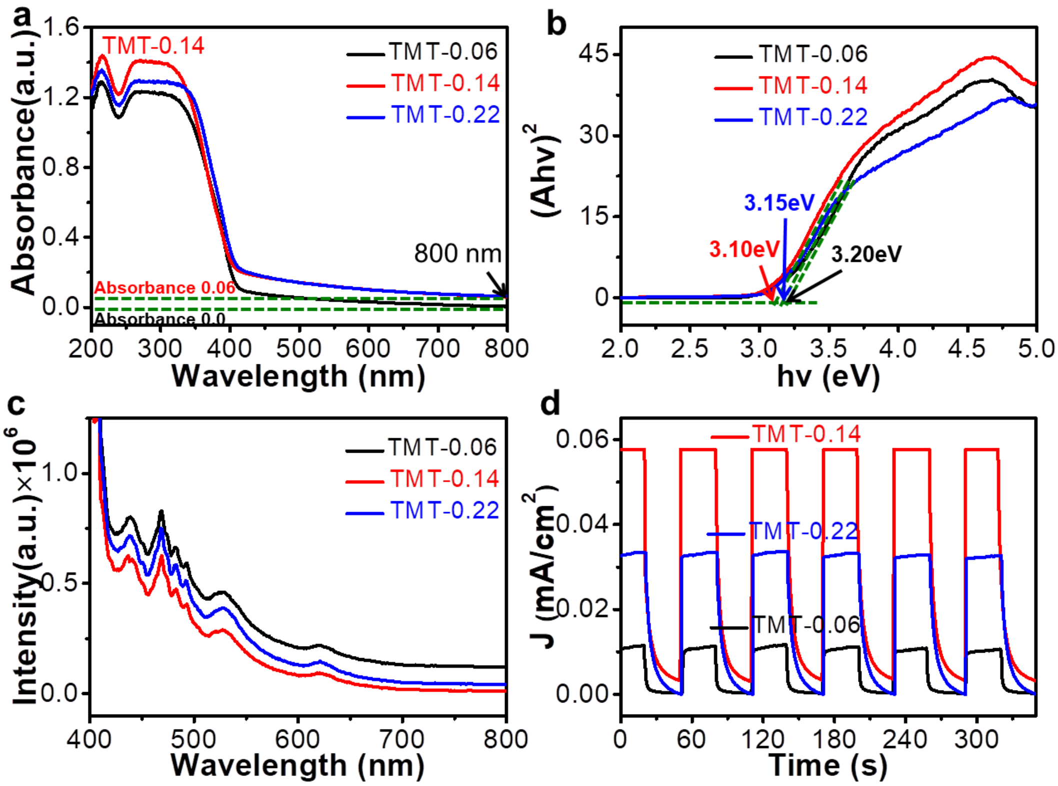
a
TMT-0.14
TMT-0.06
TMT-0.14
TMT-0.22
800 nm
Absorbance 0.06
Absorbance 0.0
Absorbance(a.u.)
Wavelength (nm)
b
TMT-0.06
TMT-0.14
TMT-0.22
3.15eV
3.10eV
3.20eV
(Ahv)^2
hv (eV)
c
TMT-0.06
TMT-0.14
TMT-0.22
Intensity(a.u.)×10^6
Wavelength (nm)
d
TMT-0.14
TMT-0.22
TMT-0.06
J (mA/cm^2)
Time (s)

Fig. 2.

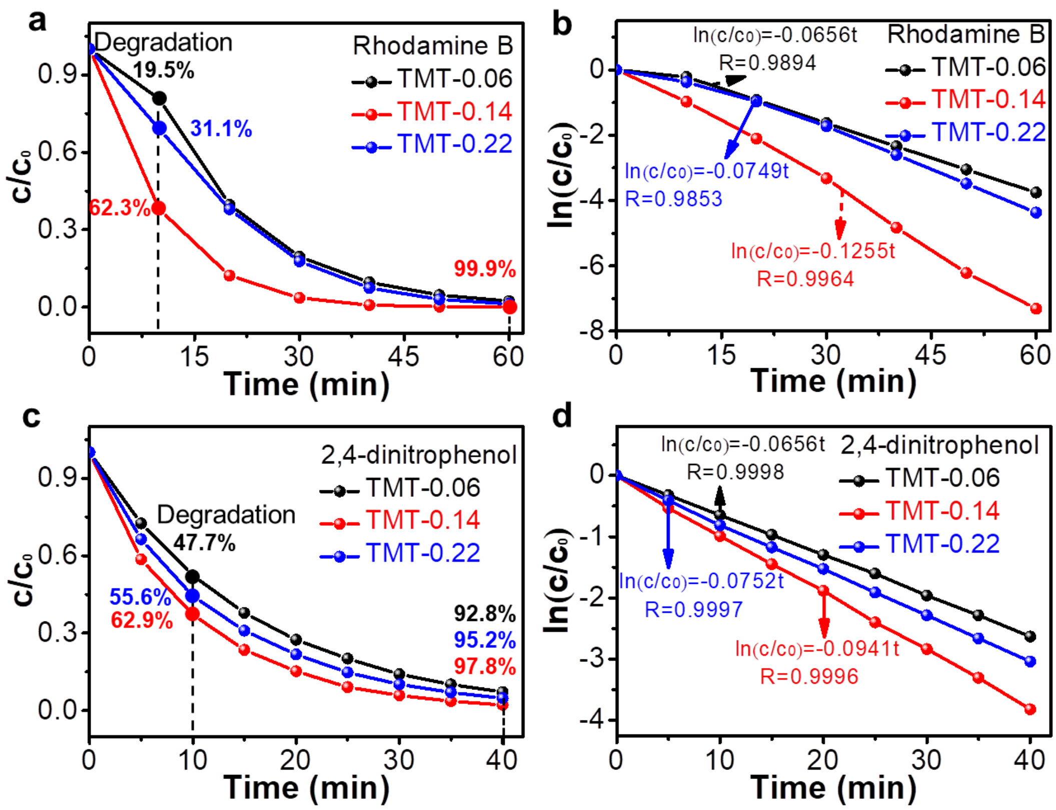
a
Degradation
19.5%
31.1%
62.3%
99.9%
Rhodamine B
TMT-0.06
TMT-0.14
TMT-0.22
c/c₀
Time (min)
b
ln(c/c₀)=-0.0656t
R=0.9894
ln(c/c₀)=-0.0749t
R=0.9853
ln(c/c₀)=-0.1255t
R=0.9964
Rhodamine B
TMT-0.06
TMT-0.14
TMT-0.22
ln(c/c₀)
Time (min)
c
2,4-dinitrophenol
TMT-0.06
TMT-0.14
TMT-0.22
Degradation
47.7%
55.6%
62.9%
92.8%
95.2%
97.8%
c/c₀
Time (min)
d
ln(c/c₀)=-0.0656t
R=0.9998
ln(c/c₀)=-0.0752t
R=0.9997
ln(c/c₀)=-0.0941t
R=0.9996
2,4-dinitrophenol
TMT-0.06
TMT-0.14
TMT-0.22
ln(c/c₀)
Time (min)

Fig. 3.

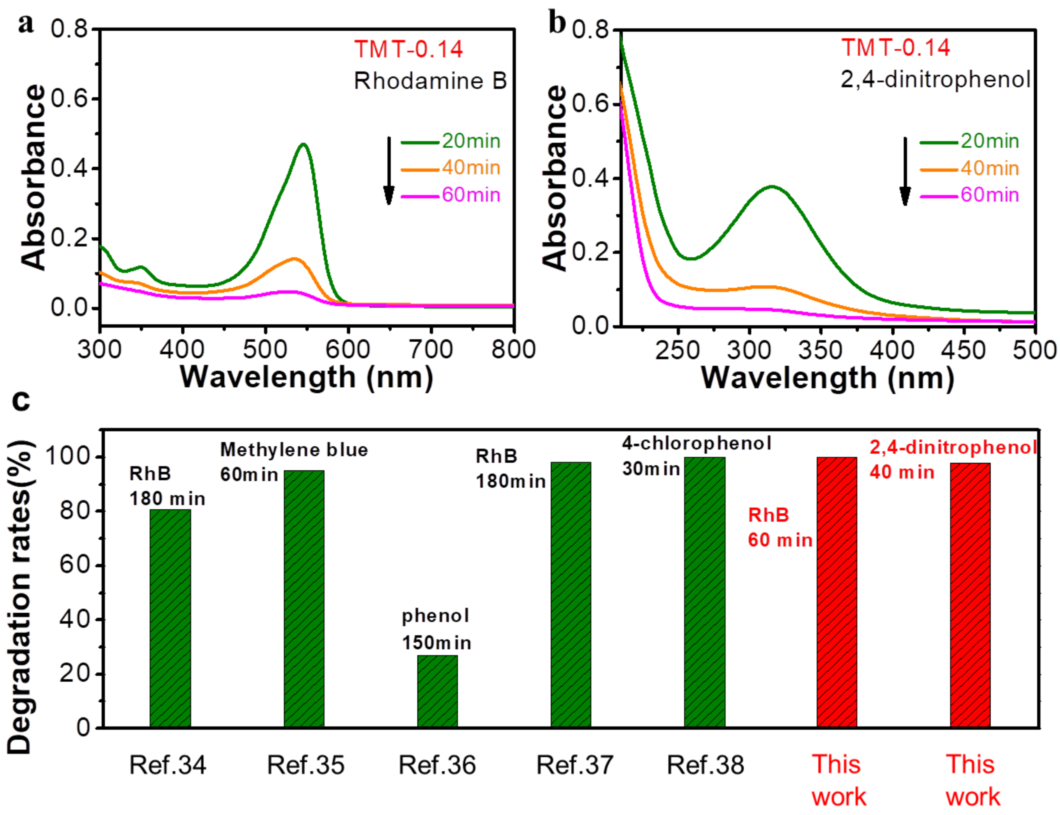
a
TMT-0.14
Rhodamine B
20min
40min
60min
Absorbance
Wavelength (nm)
b
TMT-0.14
2,4-dinitrophenol
20min
40min
60min
Absorbance
Wavelength (nm)
c
Degradation rates(%)
RhB 180 min
Methylene blue 60min
phenol 150min
RhB 180min
4-chlorophenol 30min
RhB 60 min
2,4-dinitrophenol 40 min
Ref.34
Ref.35
Ref.36
Ref.37
Ref.38
This work
This work

Fig. 4.

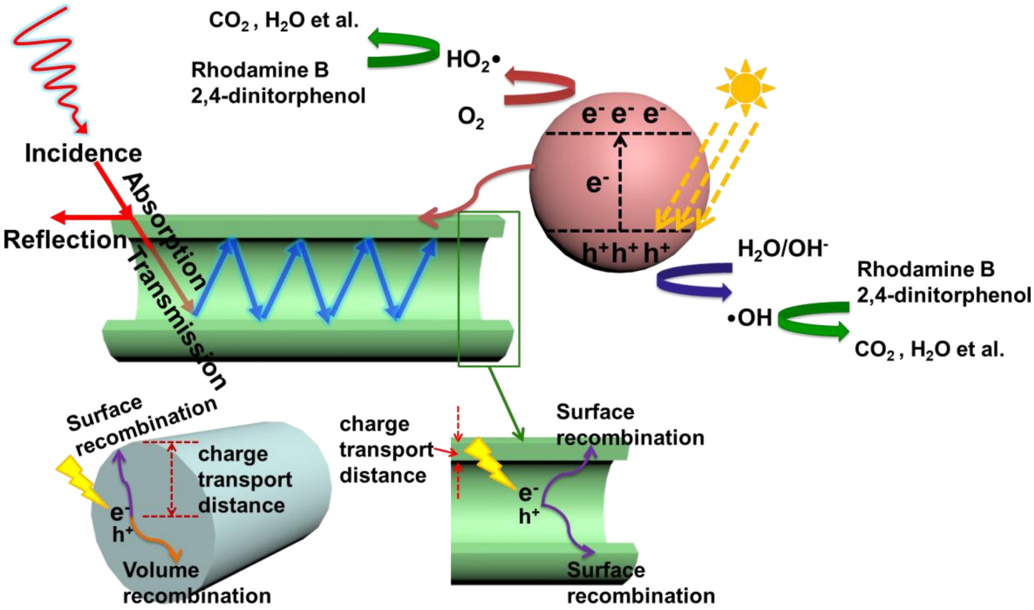

CO$_2$, H$_2$O et al.
Rhodamine B
2,4-dinitorphenol
HO$_2$•
O$_2$
Incidence
Reflection
Absorption
Transmission
e$^-$ e$^-$ e$^-$
e$^-$
h$^+$h$^+$h$^+$
H$_2$O/OH$^-$
Rhodamine B
2,4-dinitorphenol
•OH
CO$_2$, H$_2$O et al.
Surface recombination
charge transport distance
e$^-$
h$^+$
Volume recombination
charge transport distance
Surface recombination
e$^-$
h$^+$
Surface recombination

Fig. 5.

Highlights

- TiO_2 microtubes prepared by electrospinning in one step.
- The wall thickness of TiO_2 microtubes can be easily tuned by a simple method.
- The charge separation efficiency depends on the wall thickness of TiO_2 microtubes.
- The light scattering effect is strongly dependent on the size of the microtube structure.
- TiO_2 microtubes with suitable wall thicknesses have the ability to balance light-harvesting capability and charge separation efficiency.

***Declaration of Interest Statement**

Declaration of interests

☒ The authors declare that they have no known competing financial interests or personal relationships that could have appeared to influence the work reported in this paper.

☐The authors declare the following financial interests/personal relationships which may be considered as potential competing interests:

Sample CRediT author statement

Xinxin Zou: Methodology; Validation; Formal analysis; Investigation; Data Curation; Writing - Original Draft;

Yanling Yang: Supervision; Formal analysis; Investigation; Resources; Data Curation; Writing - Original Draft; Visualization

Huajun Chen: Validation; Formal analysis; Investigation

Xiao-Lei Shi: Formal analysis; Resources; Writing - Review & Editing;

Guoquan Suo: Investigation; Formal analysis

Xiaohui Ye: Formal analysis

Li Zhang: Resources

Xiaojiang Hou: Resources; Data Curation; Funding acquisition

Lei Feng: Formal analysis

Zhi-Gang Chen: Conceptualization; Resources; Writing - Review & Editing; Supervision; Project administration; Funding acquisition